Modelling of praseodymium-doped fluoride and sulfide fibre amplifiers for the 1.3 mum wavelength region

Research Report
ISSN 0167-9708
Coden: TEUEDE

Eindhoven
University of Technology
Netherlands

Faculty of Electrical Engineering

Modelling of Praseodymium-doped Fluoride and Sulfide Fibre Amplifiers for the 1.3 μm Wavelength Region

By
A.W.H. van Osch

EUT Report 95-E-294
ISBN 90-6144-294-X
October 1995

Eindhoven University of Technology Research Reports

Eindhoven University of Technology

Faculty of Electrical Engineering

Eindhoven, The Netherlands

ISSN 0167-9708 Coden: TEUEDE

MODELLING OF PRASEODYMIUM-DOPED FLUORIDE AND SULFIDE FIBRE AMPLIFIERS FOR THE 1.3 μm WAVELENGTH REGION

by

A.W.H. van Osch

EUT Report 95-E-294

ISBN 90-6144-294-X

Eindhoven

October 1995

CIP-DATA KONINKLIJKE BIBLIOTHEEK, DEN HAAG

Osch, A.W.H. van

Modelling of praseodymium-doped fluoride and sulfide fibre amplifiers for the 1.3 μm wavelength region / by A.W.H. van Osch. - Eindhoven : Eindhoven University of Technology, Faculty of Electrical Engineering. - Fig. - (EUT report, ISSN 0167-9708 ; 95-E-294)
With ref.
ISBN 90-6144-294-X
NUGI 832
Subject headings: optical fibre communication / fibre lasers / praseodymium.

Abstract

In optical communication systems, the use of optical amplifiers opens the way to an increased system performance, particularly in loss-limited long-haul systems, in dispersion limited systems and also in subscriber access systems to compensate for splitting losses. For the 1.3 μm wavelength region, the Praseodymium-doped fibre amplifier (PDFA) is a promising candidate. A numerical model is used to compare the characteristics of Pr^{3+}-doped fibres on the basis of bulk glass properties. It incorporates the distribution of the optical modes across the fibres cross-section in order to find the optimum cut-off wavelength and numerical aperture of the fibre. The model includes excited-state absorption, signal ground-state absorption and background losses. Furthermore, all forward and backward travelling noise is included. PDFAs based on sulfide glasses have a considerably improved efficiency compared to amplifiers based on ZBLAN fluoride glasses. For sulfide fibres, a numerical aperture of 0.3 is expected to be sufficient, to achieve a gain of more than 25 dB, at a pump power as low as 50 mW. For this fibre, the pump power efficiency is 0.89 dB/mW, which is a factor 6 higher than the efficiency of the ZBLAN counterpart. At 50 mW pump, a saturated output power of about 20 mW can be expected.

Keywords: Optical fibre communication, fibre lasers, Praseodymium, optical solitons, subscriber loops, CATV, computer aided analysis.

Osch, A.W.H. van
MODELLING OF PRASEODYMIUM-DOPED FLUORIDE AND SULFIDE FIBRE AMPLIFIERS FOR THE 1.3 μm WAVELENGTH REGION.
Eindhoven: Faculty of Electrical Engineering, Eindhoven University of Technology, The Netherlands, 1995. EUT Report 95-E-294.

Contact address for this research subject:
Prof. G.D. Khoe
Telecommunications Division, EH-12
Faculty of Electrical Engineering
Eindhoven University of Technology
P.O. Box 513, 5600 MB Eindhoven, The Netherlands
E-mail: G.D.Khoe@ele.tue.nl

Preface

This report describes the results of the research contribution of the Telecommunications Division of the Faculty of Electrical Engineering of Eindhoven University of Technology to the project entitled '*Optically active glass fibres*'. The project is supported by the STW (Stichting voor de Technische Wetenschappen) Technology Foundation. Within the project, new materials are being studied for efficient fibre amplifiers in the 1.3 μm wavelength region of optical telecommunications. The two research groups involved are the Glass Technology group of the Institute of Applied Physics TNO and the Telecommunications Division of the Eindhoven University of Technology. The Glass Technology group cooperates closely with the Faculty of Chemical Engineering of the Eindhoven University of Technology.

The author would like to thank STW for supporting the project, D.R. Simons for providing data on sulfide glasses and all staff members at the Telecommunications Division for the pleasant cooperation. He would also like to thank the people at Galileo Electro Optics and British Telecom for providing Pr^{3+}-doped fluoride fibres, especially M. Earnshaw of BT for making glue splices and tapered fusion splices.

Distribution list

G.A. Acket	Philips Optoelectronics Centre	The Netherlands
H. Albrecht	Siemens Central Research	Germany
W.T. Anderson	Bellcore	USA
F. Auracher	Siemens Central Research	Germany
R. Baets	University of Gent-IMEC	Belgium
A.C. van Bochove	KPN Research	The Netherlands
W. Boontje	STW Technology Foundation	The Netherlands
J.C. Bouley	CNET	France
T. Breuls	Plasma Optical Fiber	The Netherlands
B. Broberg	Industrial Microelectronics Center	Sweden
J. Buus	Gayton Photonics	UK
B. Costa	CSELT	Italy
M. van Deventer	KPN Research	The Netherlands
A. Driessen	MESA Research Institute	The Netherlands
S. Durel	CNET	France
M. Earnshaw	BT Laboratories	UK
M.S. Erman	Alcatel Alsthom Recherche	France
W.C. van Etten	University of Twente	The Netherlands
A.J. Faber	TNO Institute of Applied Physics	The Netherlands
C.F. Fernandes	Lisbon Technical University	Portugal
H.J. Frankena	Delft University of Technology	The Netherlands
N. Gisin	GAP Optique SA	Switzerland
D.C. Hall	Naval Research Laboratory	USA
J.E.M. Haverkort	Eindhoven University of Technology	The Netherlands
H. Heidrich	Heinrich-Hertz-Institut	Germany
G. Hill	BT Laboratories	UK
M.J. van der Hoek	Ingenieursbureau Coenecoop b.v.	The Netherlands
A.J.N. Houghton	RACE	Belgium
P. Jeppesen	Technical University of Denmark	Denmark
M. Karásek	Technische Universität Braunschweig	Germany
D.B. Keck	Corning Inc.	USA
A. Kersey	Naval Research Laboratory	USA
O.J. Koning	KPN Research	The Netherlands
A.M.J. Koonen	AT&T	The Netherlands

P.M. Krummrich	Technische Universität Braunschweig	Germany
A.C. Labrujere	Royal PTT Nederland N.V.	The Netherlands
V. Lagarto	CET	Portugal
C. Mahon	Tele Danmark Research	Denmark
T. Matsumoto	NTT Transmission Systems Laboratories	Japan
P. Matthijsse	PTT Telecom	The Netherlands
D. McDonald	Optronics Ireland	Rep. Ireland
H. Melchior	Institute of Quantum Electronics	Switzerland
S. Myken	RACE	Belgium
W. Nijman	Philips Optoelectronics Centre	The Netherlands
A.N. Olsson	AT&T Bell Laboratories	USA
D.N. Payne	Optoelectronics Research Centre	UK
K. Petermann	Technische Universität Berlin	Germany
J.C. van der Plaats	AT&T Network Systems Nederland	The Netherlands
J. Rawsthorne	GEC Marconi	UK
D.R. Simons	Glass Technology, Eindhoven Univ. of Techn.	The Netherlands
M.K. Smit	Delft University of Technology	The Netherlands
T. Sphicopoulos	University of Athens	Greece
A. Staring	Philips Optoelectronics Center	The Netherlands
L. Tiemeyer	Philips Optoelectronics Centre	The Netherlands
R.W. Tkach	AT&T Bell Laboratories	USA
N. Tolleshaug	Siemens A/S	Norway
B. Tromborg	Tele Danmark Research	Denmark
T. Truex	Galileo Electro Optics	USA
L. Vacha	Galileo Electro Optics	USA
B. Verbeek	Philips Research Laboratories	The Netherlands
H. de Waal	Glass Technology, Eindhoven Univ. of Techn.	The Netherlands
W. Warzannskyj	Telefonica	Spain
M. Yamada	NTT Opto-electronics Laboratories	Japan
E. Zouganeli	Telenor	Norway

Contents

1. Introduction

Optical fibre communications have replaced the traditional copper-based communication links to a large extent. Using optical fibre, huge amounts of information can be transported over very long distances. Systems are being developed for transmitting gigabits per second over a single fibre at hundreds of kilometres. Optical fibres are also being deployed in subscriber access networks for broadband services (FTTH, Fibre To The Home). Still, the fibre's capacity is not fully exploited. New techniques such as soliton transmission and OTDM (Optical Time-Domain Multiplexing) are being studied to increase transport capacity even further.

Of course, optical fibre communications are hampered by losses as well. In the past this was the main reason for the limited transmission span of fibre links, and the limited coverage of PONs (Passive Optical Networks). It was common practice to use electrical repeaters to regenerate the signal after some distance. Today, optical amplifiers have become available to boost the signal power at intermediate points. For the 1550 nm wavelength region, the EDFA (Erbium-Doped Fibre Amplifier) has conquered a predominant position. For the 1300 nm wavelength, there is an ongoing competition between fibre amplifiers and semiconductor optical amplifiers (SOA's). For this wavelength region, more research effort is required to produce an efficient fibre amplifier. There are three dopants which seem to be suitable for a 1300 nm fibre amplifier. They are Praseodymium, Neodymium and Dysprosium. For all these materials, efficiency problems are encountered. The main subject of study is to find a host glass material which produces an efficient amplifier. In semiconductor amplifiers other problems are encountered, such as polarisation dependency, coupling losses and cross-talk effects due to gain-modulation.

This report deals with the Praseodymium-Doped Fibre Amplifier (PDFA). Its principle of operation is discussed including the most relevant loss mechanisms: Multi-phonon relaxation, excited-state absorption, ground-state absorption and background loss. A computer model is developed incorporating these mechanisms. The model is used to optimise the design of Praseodymium-doped fibres. The influence of fibre geometry (cutoff wavelength, numerical aperture) on amplifier performance is studied for fluoride- and sulfide-glasses. The amplifiers behaviour under various operating conditions is investigated as well. Using these simulations a prediction of the feasible gain can be made, before efforts to fabricate the fibre.

2. Operating principle of the Praseodymium-doped fibre amplifier

The operation of Optical Fibre Amplifiers (OFA's) is based on materials which can produce optical gain. There are a few requirements that must be met. In the first place an energy gap ΔE between two electron levels in the material must exist, which matches the wavelength λ of the light that is to be amplified, by:

$$\Delta E = \frac{hc}{\lambda} \tag{2.1}$$

where c is the speed of light and h is Planck's constant. Furthermore, the transition between the two levels must be efficient. This means that a large part of the transitions that take place must produce a photon. In other words: The radiative transition rate must be large compared to the non-radiative rate. In the third place there must be a way to populate the upper of the two levels by pumping the amplifier with a lightsource of a shorter wavelength.

Some rare-earths doped in a glass host appear to have these properties. For the 1550 nm window, Erbium is being used successfully. For 1310 nm Praseodymium, Neodymium and Dysprosium are being studied. For Neodymium there is a strong excited-state absorption (ESA) and a competing emission transition at 1.05 μm. Glass materials are being studied with reduced ESA. Furthermore, measures are taken to filter the ASE at 1050 nm. Dysprosium is a very promising material because it enables the use of shorter fibres. For Praseodymium, research concentrates on the development of a glass host with a low phonon energy to improve the quantum efficiency.

2.1 Energy levels of Praseodymium in a glass host

To discuss the operation of the PDFA, we must take a close look at the energy level diagram of Praseodymium in a glass host (Fig. 2.1). The energy levels of Praseodymium are no longer sharp lines if it is doped in a glass host, due to Stark splitting and homogeneous broadening. The ${}^1G_4$ - ${}^3H_5$ transition is responsible for signal amplification. The transition can be induced by other photons with the same energy, to produce stimulated emission. Inevitably, the transition will also take place spontaneously. Just like the signal, this spontaneous emission will be amplified, producing ASE (Amplified Spontaneous Emission). From the ${}^3H_5$ level, electrons rapidly fall to the ${}^3H_4$ level. The energy is lost as heat, by phonon emission. To enable a $^1G_4$ - $^3H_5$ transition, the $^1G_4$ level (excited state) has to be populated first, by pumping the amplifier. Pump photons are absorbed by the $^3H_4$ ground state to the $^1G_4$ state. The energy gap of this transition is larger, corresponding to a shorter wavelength. The $^3H_5$ - $^3H_4$ transition is so strong, compared to the other two, that the population density of the $^3H_5$ level can be neglected. This means that the ion quickly becomes available for the next amplification cycle.

Apart from these fundamental transitions which are responsible for amplification, other transitions take place. Firstly, the $^1G_4$ level shows a non-radiative decay. By multi-phonon relaxation, electrons from the $^1G_4$ level can fall to the $^3H_4$ ground state either directly or via one or more of the $^3F_4$, $^3F_3$, $^3F_2$, $^3H_6$ or $^3H_5$ levels. The lifetime of the $^1G_4$ level is called the spontaneous emission lifetime τ. This is the time in which the population falls to 1/e of its original value. Multi-phonon relaxation is the main problem in Pr^{3+}-doped fibre amplifiers. It is responsible for the very low quantum efficiency (defined as the number of 1.3 μm photons emitted over the number of pump photons absorbed) of fluoride amplifiers.

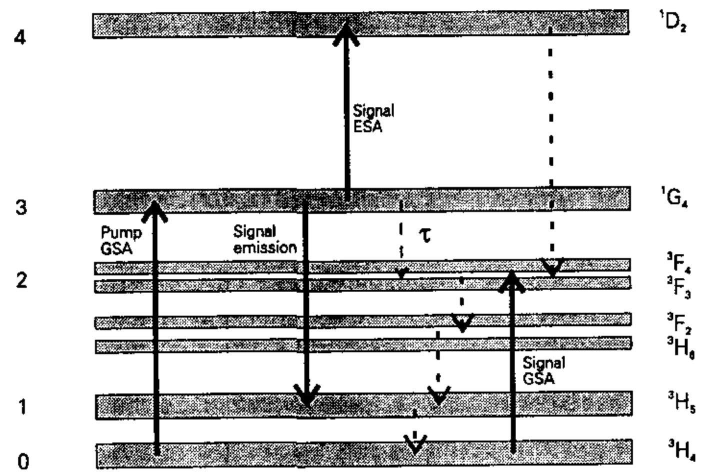

Fig. 2.1: Energy levels of Pr^{3+} in a glass host

Not all electrons from the $^1G_4$ level will make a transition to a lower energy level. There exists a transition to the higher $^1D_2$ level, which has an energy gap that corresponds more or less to the $^1G_4$ - $^3H_5$ gap. A signal photon can therefore not only lead to stimulated emission but can be absorbed by an electron in the excited state as well. The photon will be lost, leading to a decreased gain. This effect is called excited-state absorption (ESA). From the $^1D_2$ level, the majority of electrons will subsequently fall non-radiatively to the $^3F_4$ / $^3F_3$ levels. ESA will thus lead to a depopulation of the excited state, degrading the amplifiers gain even further.

Another loss mechanism is the signal ground-state absorption (GSA). Photons can be absorbed from the ground state to the $^3F_3$ / $^3F_4$ levels. They will rapidly fall back to the ground state, but a photon will be lost anyway. Of course, GSA can only occur if there are any electrons in the ground state. If the population is inverted the ground-state absorption will be bleached.

The previously discussed loss mechanisms were all caused by electron transitions within the Praseodymium ions. Just like in ordinary transmission fibres, light will also be lost by scattering against impurities within the glass and by absorption of various chemical bonds e.g. the O-H bond. In doped fibres, these losses are generally much higher. It is difficult to obtain the high-purity starting materials for the glass composition as well as for the dopant. Good Pr^{3+}-doped fibres still have a background loss of 0.1 - 0.5 dB/m, hundreds of times more than transmission fibres. Fortunately, only limited lengths are needed for a practical amplifier.

2.2 Cross-section data on Pr^{3+} in ZBLAN- and sulfide-glasses

The level transitions that were discussed in the previous section can be completely characterised by their cross-section spectra and spontaneous emission lifetimes. The spontaneous decay from a certain level I, is given by the constant τ_I. This constant is determined by all radiative and non-radiative decay channels starting from level I. The cross-section is a measure of the strength of an induced transition at a certain wavelength. The stimulated transition rate W_{IK} between levels I and K can be expressed as [1]:

$$W_{IK}(x,y,z) = \int_0^\infty \sigma_{IK}(\nu)\frac{I(\nu,x,y)}{h\nu}P(\nu,z)\ \mathrm{d}\nu \tag{2.2}$$

where $\sigma_{IK}(\nu)$ is the cross-section involved. $P(\nu,z)$ is the optical power spectral density [W/Hz] over the fibre's cross-section. $I(\nu,x,y)$ is the transverse intensity distribution of the optical mode at frequency ν, normalised to:

$$\iint I(\nu,x,y)\,\mathrm{d}x\,\mathrm{d}y = 1 \tag{2.3}$$

From (2.2) it is clear that the transition rate at a certain point within the fibre is proportional to the product $P(\nu,z)\ I(\nu,x,y)$, which is the optical power spectral and spatial density [Ws/m^2]. Before integration, each frequency is scaled with $\sigma_{IK}(\nu)$. One can thus think of the cross-section as the ion's statistical likelihood of absorbing or emitting a photon.

In fig. 2.2 cross-section data determined from measurements on ZBLAN hosts are shown [2], [3]. The stimulated emission cross-section peaks at 1.33 μm. At this wavelength the stimulated emission appears to be most efficient. Maximum gain however, will be obtained at a shorter wavelength. This is due to the tail of the excited-state absorption cross-section starting at approximately 1.29 μm. In the previous section it was argued that ESA is a loss mechanism. The balance between stimulated emission and ESA will therefore determine the gain. The ground-state absorption cross-section is also shown in Fig. 2.2. The GSA has a wide short-wavelength tail as well. The lifetime of the $^1G_4$ level was found to be 110 μs. The peak of the pump absorption cross-section occurs at 1017 nm and has a value of 4.3 10^{-26} m^2.

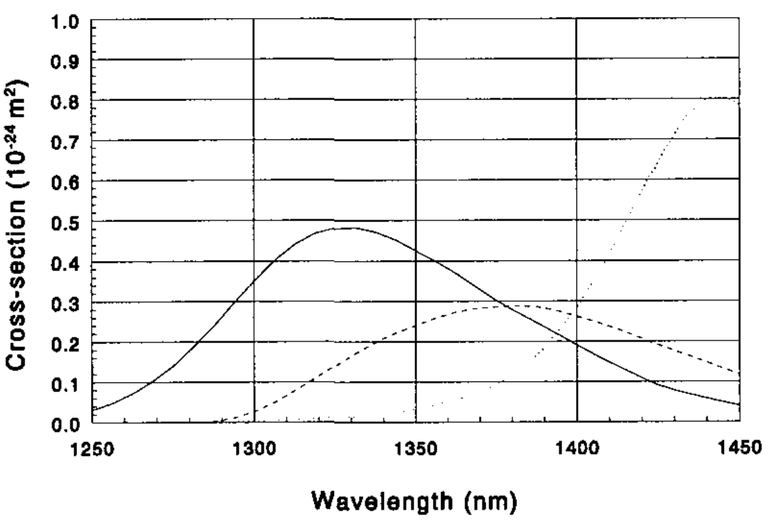

Fig. 2.2: Cross-sections for ZBLAN. Signal stimulated emission (solid line), signal excited-state absorption (dashed line), signal ground-state absorption (dotted line)

The quantum efficiency of Pr^{3+}-doped ZBLAN-glasses appears to be disappointing. A value of 3.4% was reported [4]. This is due to the fact that (non-radiative) multi-phonon relaxation dominates the decay of the $^1G_4$ level. New host materials are being studied to improve the quantum efficiency. Sulfide-glasses are reported by Simons [5,6], with considerably enhanced performance. In fig. 2.3 cross-sections are shown of the $(GeS_3)_{80}(Ga_2S_3)_{20}$ sulfide-glass. The stimulated emission cross-section is larger than the cross-section of ZBLAN. The ESA is very strong but is shifted towards longer wavelengths, making it less harmful. Furthermore the lifetime was increased to 360 μs. The GeGaS-glass has a calculated quantum efficiency of 59% at 1310 nm. The pump absorption has its peak (9.7 10^{-26} m^2) at 1026 nm. The optimum pump wavelength is shifted about 10 nm, but it should be no problem to design InGaAs laser diodes for this wavelength.

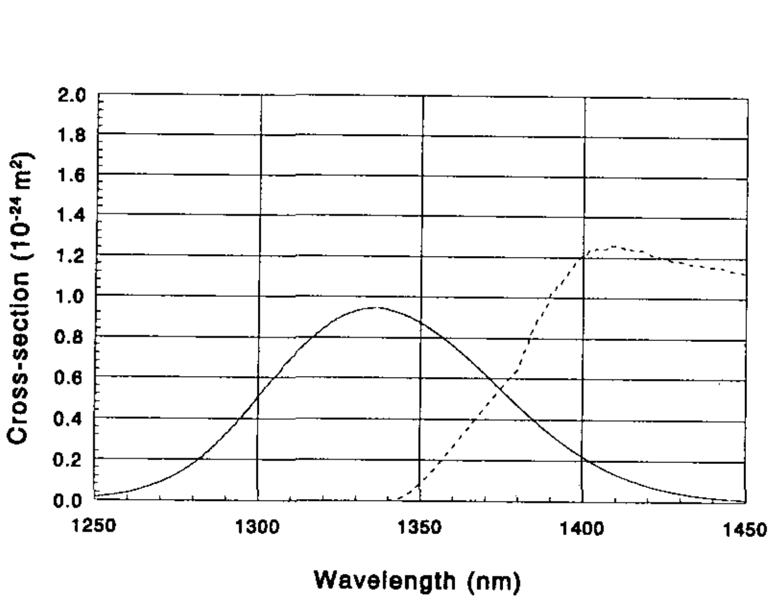

Fig. 2.3: Cross-sections for GeGaS. Signal stimulated emission (solid line), signal excited-state absorption (dashed line), signal ground-state absorption (dotted line)

2.3 Amplifier configurations

From the previous sections it is clear that the signal and pump powers must both be fed to the same praseodymium-doped fibre. Because the pump and signal wavelengths differ, a WDM fibre multiplexer can be employed to combine both powers, in principle without any losses. In fig. 2.4 a simple co-propagating pumping scheme is shown. This means that the signal and pump beams pass the Pr^{3+}-doped fibre in the same direction. The pump module consists of two polarisation multiplexed laser diodes. In this way both powers can be combined, in principle without any loss. The combined pump and signal beams are fed to the doped fibre using two special splices. A glue splice is used, as it is not possible to connect silica fibres to fluoride or sulfide fibres by fusion splicing. Pump efficient praseodymium-doped fibres have a small core diameter and a high NA as compared to standard transmission fibres (see chapter 4). This results in a much lower mode field diameter (MFD) of the pump and signal modes. A Thermally diffused Expanded Core (TEC) is used to splice a high-NA fibre to the standard fibre [7]. Using this technique it is possible to obtain a locally increased MFD. The coupling losses can be drastically reduced in this way. Using the above configuration, a pump power efficiency of 0.21 dB/mW was achieved using a fluoride fibre [4]. The gain was 17 dB at 100 mW pump.

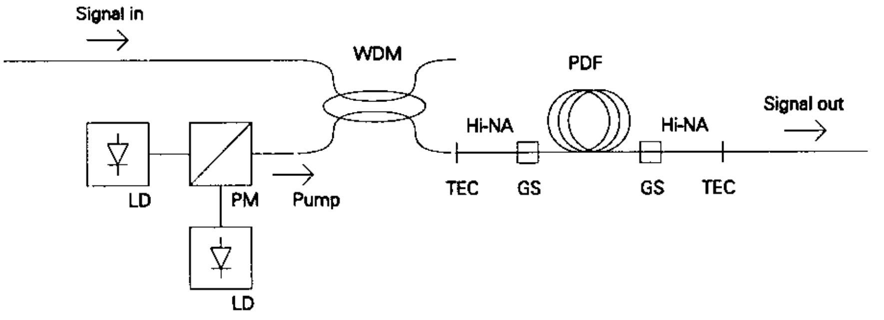

Fig. 2.4: Co-propagating amplifier configuration. WDM: Wavelength Division Multiplexer, LD: Laser Diode, PM: Polarisation Multiplexer, TEC: Thermally-diffused Expanded Core splice, Hi-NA: High-NA fibre, GS: Glue Splice, PDF: Praseodymium-Doped Fibre

Optical fibre amplifiers can also be pumped in the opposite direction of the signal beam. This configuration is depicted in fig. 2.5. It has the advantage that no residual pump power is present in the output fibre. It will however enter the input fibre if no isolator is used. Counter-pumped fibre amplifiers can have a slightly higher gain but generally the noise characteristics are worse. For a low-noise amplifier a high gain is required at the signal input. Therefore a co-propagating configuration is in favour.

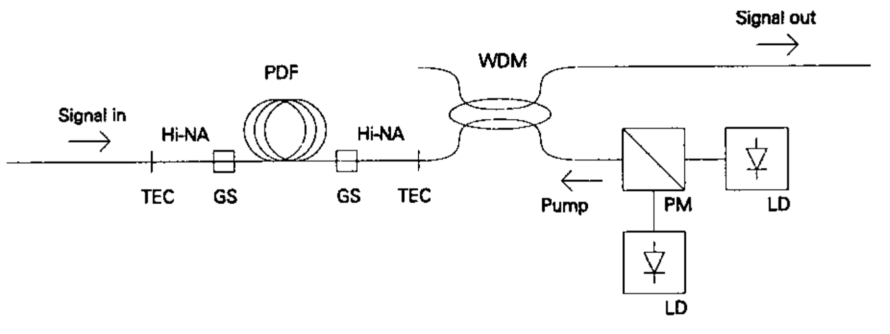

Fig. 2.5: Counter-propagating amplifier configuration. WDM: Wavelength Division Multiplexer, LD: Laser Diode, PM: Polarisation Multiplexer, TEC: Thermally-diffused Expanded Core splice, Hi-NA: High-NA fibre, GS: Glue Splice, PDF: Praseodymium-Doped Fibre

The previously discussed configurations can be combined as well. This is the bi-directional configuration of fig. 2.6. Using this configuration, the coupled pump power is doubled, producing a much higher gain. Another advantage is that the residual pump powers enter neither the input fibre nor the output fibre. By the second WDM it is coupled to the other pump module. Care must be taken that the residual pump powers are not too high, as the pump lasers may become unstable or even be damaged.

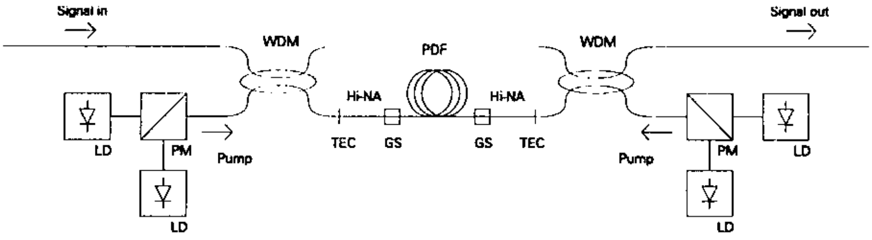

Fig. 2.6: Bi-directional amplifier configuration. WDM: Wavelength Division Multiplexer, LD: Laser Diode, PM: Polarisation Multiplexer, TEC: Thermally-diffused Expanded Core splice, Hi-NA: High-NA fibre, GS: Glue Splice, PDF: Praseodymium-Doped Fibre

In [4] an increased pump power efficiency of 0.24 dB/mW was reported using this setup. At 100 mW pump power, a gain of 22 dB was obtained at 1.3 μm.

In [8] a double path configuration is suggested. Here the signal is reflected back at the output side of a bi-directionally pumped amplifier. At the input side it is split from the incoming signal using an optical circulator. In this way the signal will pass the Pr^{3+}-doped fibre twice. The gain will therefore be doubled. This of course only applies to the small-signal regime. If the amplifier saturates, the output power will be limited by the available pump power.

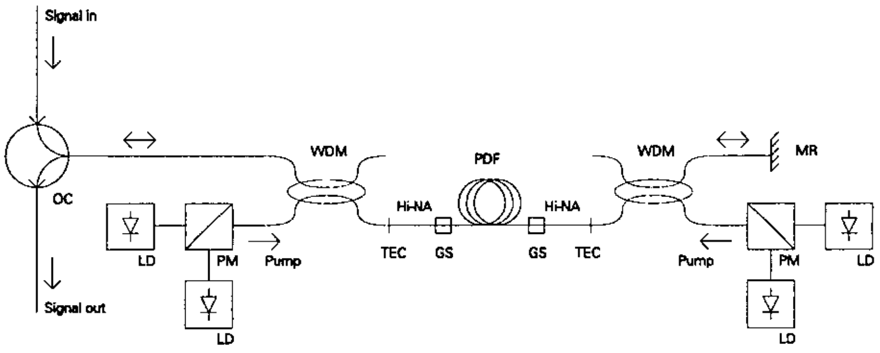

Fig. 2.7: Double-path amplifier configuration. WDM: Wavelength Division Multiplexer, LD: Laser Diode, PM: Polarisation Multiplexer, TEC: Thermally-diffused Expanded Core splice, Hi-NA: High-NA fibre, GS: Glue Splice, PDF: Praseodymium-Doped Fibre, OC: Optical Circulator, MR: Mirror

Using the double-path configuration, 0.4 dB/mW pump power efficiency was obtained [8]. To achieve a 25 dB gain, the LD drive current could be decreased by 42% compared to the single-path configuration. As a result, the lifetime of the pump lasers is expected to be substantially higher.

The PDFA can be used at different locations within an optical fibre link. Firstly, it can be used as pre-amplifier at the receiver side to increase receiver sensitivity. In this case the input signal power will be very low. It is also possible to use the amplifier as in-line amplifier at one or more places within a long link. Again, the input power is generally quite low. If the PDFA is placed at the transmitter side however, the input power can be up to several milliwatts. Here, the amplifier will saturate. That is why the double-path configuration is useless here.

3. Modelling of the Praseodymium-doped fibre amplifier

In a Pr^{3+}-doped fibre amplifier, various possibilities in the electronic transitions determine the amplifier characteristics. These transitions have already been discussed in chapter 2. In this chapter, equations will be derived for a comprehensive model, which can be used to study the amplifiers operation at different operating regimes. It can be used to optimise the design of Praseodymium-doped fibres as well. The resultant model has to be solved on a computer system employing numerical methods. It is spectrally as well as spatially resolved and includes signal ground-state absorption, signal excited-state absorption and background losses.

3.1 Basics of fibre amplifier modelling

In the past, a lot of attention has been paid to the modelling of Er-doped fibre amplifiers. Very accurate results have been found and the models are successfully being used for the design of Erbium-doped fibres and the evaluation of systems incorporating EDFAs. The amplifier system for PDFAs is more complex because more transitions are involved. The level structure of Fig. 2.1 is used as a basis for the model.

Results from EDFA modelling [9] showed an error in the gain at high pump powers. It was later confirmed that this was due to saturation of the amplifier by ASE. Using a spectrally resolved model, a close agreement was obtained between simulations and measurements. It was clear that ASE contributions at all wavelengths must be taken into account. This will apply to Praseodymium-doped fibre amplifiers as well. In fig. 3.1 an example of an ASE spectrum at the output of a PDFA is shown. The wavelength range where appreciable noise is generated, is subdivided into a number of sections. For each section, the optical power versus distance within the fibre has to be calculated. The range λ_{min} - λ_{max} depends on the glass substance. It can be estimated from the emission and ESA cross-section spectra. λ_{min} is chosen at the onset of the emission spectrum and λ_{max} is taken at the crossing of the emission and ESA cross-section spectra.

In the development stage of praseodymium-doped fibres, the optimum fibre structure is to be determined with the aid of the model. There are basically three parameters which can be varied. These are the fibre's numerical aperture (*NA*), cut-off wavelength (λ_c) and the dopant distribution. The core radius (a) is related to this by:

$$a = \frac{2.405\,\lambda_c}{2\pi NA} \tag{3.1}$$

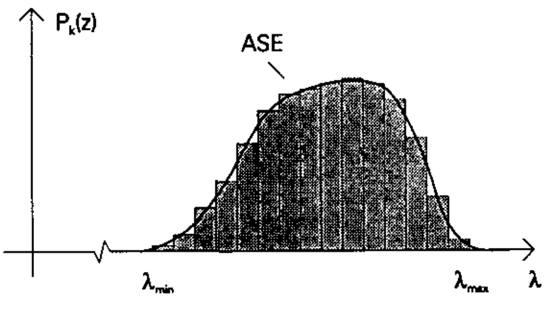

Fig. 3.1: Noise spectrum at amplifier output

In the simplest fibres the dopant distribution is uniform across the fibre core cross-section. If the dopant is mainly centred around the axis of the core, the fibre's gain efficiency can possibly be further increased. This is a result of the high intensity of the pump and signal modes in the proximity of the fibre axis. To find the optimum fibre structure, the mode profiles of pump and signal must be evaluated. The core area of the fibre is subdivided in a number of concentric rings (Fig 3.2). For each ring the optical intensities of pump, signal and all ASE-sections are calculated using the total powers and the mode profiles.

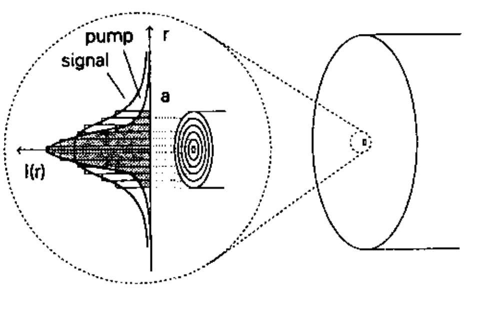

Fig. 3.2: Pump and signal mode profiles

From the considerations above it is concluded that a three-dimensional problem is to be solved. A discretisation is needed in wavelength, radius and distance within the fibre. In the following section the set of equations that is required for this will be discussed.

3.2 Rate equations and propagation equations

For the evaluation of optical powers in a fibre amplifier, two types of equations are required. Firstly, the so-called rate-equations are used which describe the transition rates between the various levels in the doped material. Secondly, the propagation equations are used to model the evolution of optical powers versus travelled distance. The transition rates are in accordance with (2.2). The pump absorption rate is:

$$W_{03}(r,z) = \sigma_{03}(\nu_p)\frac{P_p^+(z)+P_p^-(z)}{h\nu_p}I(r,\nu_p) \tag{3.2}$$

Where $\sigma_{03}(\nu_p)$ is the pump absorption cross-section at the pump frequency ν_p. Integration over ν is not required, as the pump is assumed to have one single wavelength. $P_p^+(z)$ is the pump power that is propagating in the forward direction. $P_p^-(z)$ is the counter-propagating pump power. The excited-state absorption rate due to signal and ASE powers is given by:

$$W_{34}(r,z) = \int_{c/\lambda_{min}}^{c/\lambda_{max}} \sigma_{34}(\nu)\frac{P_{ase}^+(z,\nu)+P_{ase}^-(z,\nu)}{h\nu}I(r,\nu)\,d\nu + \sigma_{34}(\nu_s)\frac{P_s(z)}{h\nu_s}I(r,\nu_s) \tag{3.3}$$

Here, a single-wavelength signal is assumed. $\sigma_{34}(\nu)$ is the excited-state absorption cross-section. ν_s is the signal frequency, $P_{ase}^+(z,\nu)$ and $P_{ase}^-(z,\nu)$ are the forward and backward propagating noise power spectral densities. $P_s(z)$ is the signal power. The noise (ASE) is integrated over the wavelength range λ_{min} - λ_{max}. Finally, the stimulated emission rate follows from a similar equation, using the stimulated emission cross-section $\sigma_{31}(\nu)$:

$$W_{31}(r,z) = \int_{c/\lambda_{min}}^{c/\lambda_{max}} \sigma_{31}(\nu)\frac{P_{ase}^+(z,\nu)+P_{ase}^-(z,\nu)}{h\nu}I(r,\nu)\,d\nu + \sigma_{31}(\nu_s)\frac{P_s(z)}{h\nu_s}I(r,\nu_s) \tag{3.4}$$

The transition rate for signal ground-state absorption does not need to be evaluated as the ions rapidly fall back to the ground-state. Only the transitions that effect the population inversion are needed. For equations (3.2) to (3.4), the normalised intensity in the fibre core is calculated as [10]:

$$I(r,\nu) = \frac{1}{\pi}\left[\frac{\upsilon}{aV}\frac{J_0(ur/a)}{J_1(u)}\right]^2 \tag{3.5}$$

where J_0 and J_1 are the zero order and first order Bessel functions of the first kind. The V-number at wavelength λ (= c/ν) is:

$$V = \frac{2\pi a}{\lambda} NA \tag{3.6}$$

The value of υ can not be calculated analytically. It is found by interpolation from a table given in [11]. A linear approximation is often used to find υ, but this is not accurate for small values of V. u is related to V and υ by:

$$u = (V^2 - \upsilon^2)^{1/2} \tag{3.7}$$

In the steady-state situation, an equilibrium will be reached between the various transition rates. This means that the population densities of levels 0 and 3 will no longer change. Given this, expressions can be derived for the population densities of both levels:

$$\eta_3(r,z) = \rho(r)\frac{W_{03}(r,z)}{W_{03}(r,z)+W_{34}(r,z)+W_{31}(r,z)+1/\tau} \tag{3.8}$$

$$\eta_0(r,z) = \rho(r) - \eta_3(r,z) \tag{3.9}$$

$\eta_3(r,z)$ and $\eta_0(r,z)$ are the densities of Pr^{3+}-ions in the $^1G_4$ and $^3H_4$ states, respectively. $\rho(r)$ is the total density of Pr^{3+}-ions and τ is the spontaneous emission lifetime. When the population densities (and population inversion) are known, the propagation of pump, signal and ASE can be determined. In [12] propagation equations are given for PDFAs. Here, the signal ground-state absorption is incorporated by a factor $\alpha(\nu)$, which is independent of the population inversion. This is not correct. The signal ground state absorption of a PDFA should be included in the model as a population-inversion dependent factor, as it is bleached in an inverted amplifier. We will introduce a new ground-state absorption factor $g_g(z,\nu)$, and use $\alpha(\nu)$ for the background loss, which is indeed independent of the population inversion. The equations become:

$$\frac{dP_p^{\pm}(z)}{dz} = \mp[g_p(z)+\alpha(\nu_p)]\,P_p^{\pm}(z) \tag{3.10}$$

$$\frac{dP_s(z)}{dz} = [g_e(z,\nu_s)-g_a(z,\nu_s)-g_g(z,\nu_s)-\alpha(\nu_s)]\,P_s(z) \tag{3.11}$$

$$\frac{dP_{ase}^{\pm}(z,\nu)}{dz} = \pm[g_e(z,\nu)-g_a(z,\nu)-g_g(z,\nu)-\alpha(\nu)]\,P_{ase}^{\pm}(z,\nu) \pm 2h\nu\Delta\nu\, g_e(z,\nu) \tag{3.12}$$

$\Delta\nu$ is the bandwidth of the wavelength section being considered. The pump ground-state absorption, signal/ASE stimulated emission, signal/ASE excited-state absorption and signal/ASE ground-state absorption factors are given by:

$$g_p(z) = 2\pi\sigma_{03}(\nu_p)\int_0^a \eta_0(r,z)\,I(r,\nu_p)\,r\,dr \tag{3.13}$$

$$g_e(z,\nu) = 2\pi\sigma_{31}(\nu)\int_0^a \eta_3(r,z)\,I(r,\nu)\,r\,dr \tag{3.14}$$

$$g_a(z,\nu) = 2\pi\sigma_{34}(\nu)\int_0^a \eta_3(r,z)\,I(r,\nu)\,r\,dr \tag{3.15}$$

$$g_g(z,\nu) = 2\pi\sigma_{02}(\nu)\int_0^a \eta_0(r,z)\,I(r,\nu)\,r\,dr \tag{3.16}$$

The background loss $\alpha(\nu)$ is expressed in Np/m (1 Neper = 4.34 dB).

3.3 Numerical solution of differential equations

The equations of section 3.2 can not be solved analytically. Numerical methods are required to find an approximate solution. Equations (3.10) to (3.12) must be integrated to find the pump, signal and ASE powers versus the distance within the fibre. Equation (3.10) are actually two equations, one for the co-propagating and one for the counter-propagating pump power. Equation (3.12) has to be solved for each wavelength section of the ASE spectrum and for both directions of propagation. The number of ASE sections determines the accuracy at which the total ASE power is evaluated. In an amplifier that is saturated by ASE, it is important to find the ASE spectrum as accurately as possible. Because the cross-section spectra are quite smooth, no great number of sections are required. For the simulations discussed in following chapters, only five were used. No substantial changes were observed for a higher number of sections.

The boundary values which apply to the set of equations are straightforward. For the pump power we have $P_p^+(0) = \gamma P_{p,in}$ and $P_p^-(L) = (1-\gamma) P_{p,in}$, where γ is the fraction of pump power that is applied in the co-propagating direction. For the signal we have $P_s(0) = P_{s,in}$, and the boundary conditions for the noise are $P_{ase}^+(0) = 0$ and $P_{ase}^-(L) = 0$.

For each integration step of (3.10) to (3.12), equations (3.13) to (3.16) have to be evaluated first. For this, the population densities of (3.8) and (3.9) are required. To find these, the transition rates of (3.2) to (3.4) are calculated. In the latter equations, all signal, pump and ASE powers are being used. This completes the circle. To find a solution for one of the differential equations, the solutions of all other equations must be known. This means that the equations are coupled. We have a set of simultaneous differential equations. Another problem is the fact that boundary values are given at two points. The forward propagating powers have boundary conditions at z=0, whilst boundary conditions apply at z=L for the backward beams. If the equations are integated in the forward direction, a guess must be made for the powers of the counter-propagating beams at z=0.

In our simulation program, a Newton iteration technique is used to make a new guess solution before each integration. The full set of equations is integrated over and over again until the solution of all equations stabilises. The number of iterations that is required depends on the specific conditions of the simulation and the initial guess that is used. In some conditions the iteration may not converge at all and the routine will terminate with an error. The program is written in Fortran. It was compiled and run on a SGI Power Challenge XL supercomputer, to yield reasonable computing times. At first, tables of material properties and fibre parameters must be loaded. When the operating conditions are set, a simulation run can be performed. This includes simulations versus the fibre's geometrical parameters to determine the optimum fibre structure. Results can be plotted on the screen or to a file in postscript format. It is also possible to write the results to a file in table form.

3.4 Verification of simulation results

The computer program was verified with results from measurements for two reasons. Firstly, it must be checked that the model was correctly translated into a computer algorithm and that this algorithm was correctly programmed. Secondly, an indication of the validity of the model can be obtained. We used results from measurents on a 2000 ppmwt Pr-doped ZBLAN fibre [13]. The cut-off wavelength of the fibre is 1.26 μm and it has an NA of 0.41. The fibre length is 8 meters.

In Fig. 3.3 small-signal gain measurements are shown versus pump power (circles). The signal wavelength was 1.31 μm. The results were found by adding 6 dB to the measured gain [3]. This is the loss of the unpumped fibre. Simulation results of our computer model are also shown in the figure. These are the results for the actual gain, not corrected to zero for the unpumped case. It can be seen that the unpumped fibre indeed has a loss of about 6 dB at P_p = 0. When 6 dB is added to the simulation results, it is in good agreement with the measurements.

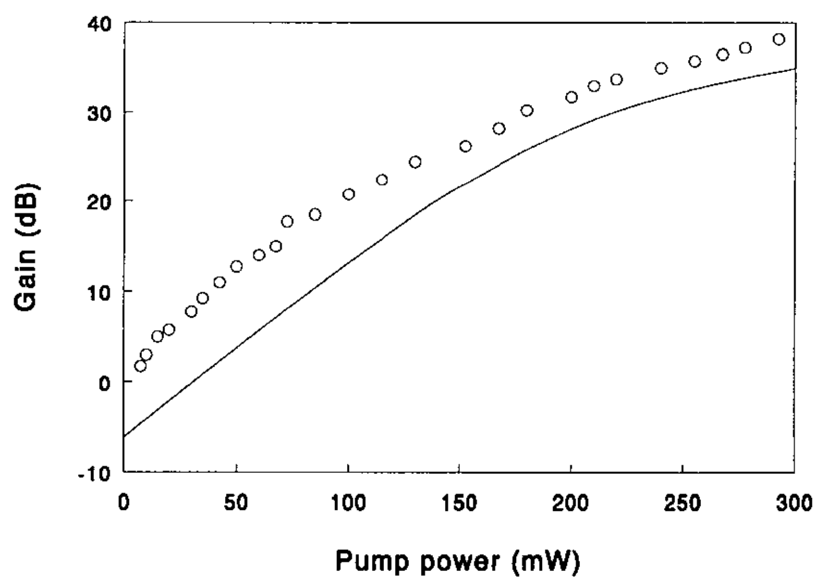

Fig. 3.3: Gain versus pump power. Gross gain, measured (circles). Net gain, simulated (line).

Next, a simulation versus signal wavelength was carried out using the same fibre parameters. Results are depicted in fig. 3.4. The pump power is 300 mW. Again the result of [13] is not the actual gain of the amplifier but the difference between the pumped and unpumped situation. To take this into account, two simulation runs were carried out, one with the pump power on (dashed curve) and one with the pump switched off (dotted curve). When these two are subtracted, we find the solid curve which is in agreement with the measurements.

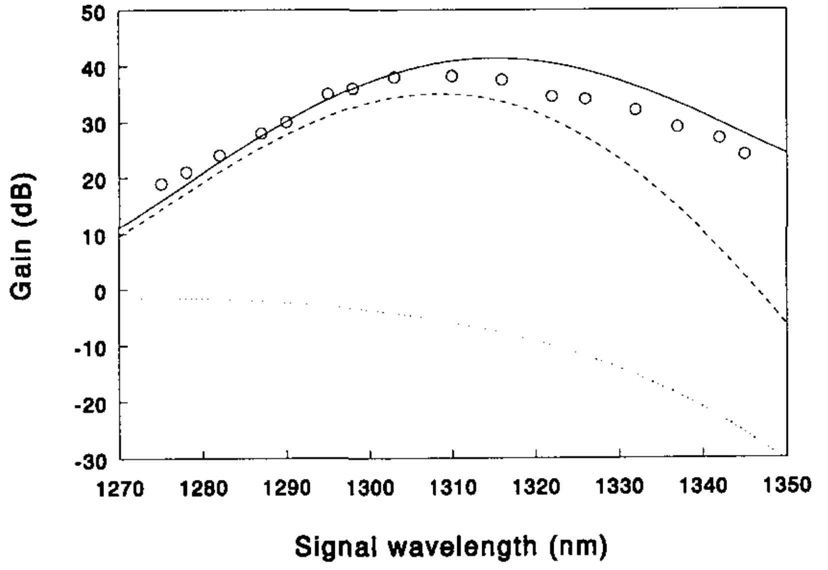

Fig. 3.4: Gain versus signal wavelength. Gross gain, measured (circles). Gross gain simulated (solid). Simulation pumped amplifier (dashed). Simulation unpumped amplifier (dotted)

4. Design of Praseodymium-doped fibres

The principle of operation of the Praseodymium-doped fibre amplifier was discussed in chapter 2. This was a qualitative approach. No insight has yet been gained in the efficiency of the amplification mechanism. This depends on a large number of factors, such as location and concentration of the dopant and the intensity and the length of interaction between the light beams and the dopant. The model of chapter 3 will be used to study the influence of the fibre parameters. This will lead to an optimum design of the praseodymium-doped fibre yielding a maximum efficiency.

4.1 Dopant concentration and distribution

The concentration of the Pr-dopant is generally expressed in ppmwt (mg/kg). In principle, one would like to have the dopant concentration as high as possible. This would lead to very short lengths of the fibre, which is an advantage in view of practical use and costs. Furthermore, the amplifier would be less hampered by the fibre background loss. Unfortunately, this is not possible. If the concentration is chosen too high, the average distance between two adjacent Praseodymium ions becomes too small. If two dopant atoms are in close proximity, energy can be transferred between the two. This effect is called co-operative upconversion. In this process an atom in the $^1G_4$ level can fall to the $^3H_5$ state (Fig. 2.1), simultaneously exciting the neighbour to the $^1D_2$ level. Co-operative upconversion leads to an increased non-radiative decay rate from the $^1G_4$ level, so the spontaneous emission lifetime of this level will decrease. In [14] it was shown that co-operative upconversion degrades ZBLAN amplifier performance at concentrations of 1000 ppmwt or more. A concentration of 500 ppmwt Pr^{3+} is a good value for efficient amplifiers.

Normally the dopant is uniformly distributed in the fibre core. It is also possible to confine the dopant to a certain region close to the fibre axis. As was shown in [1], the device efficiency may be improved for Er^{3+}-doped SiO_2 fibres because of a better inversion. Dopant confinement will have to be compensated by using longer fibres. Due to the relatively high background loss of ZBLAN fibres, confinement of the Er^{3+}-dopant results in a decreased gain. The same goes for Pr^{3+}-doped ZBLAN fibres and probably also for Pr^{3+}-doped sulfide fibres. Throughout the rest of this report only the uniform dopant distribution will be considered.

4.2 Optimum cut-off wavelength

The fibre geometry, relevant to optical propagation, can be described in full using two parameters. We can use the core radius and the refractive index difference between the core and the cladding. It is common practice however, to use the cut-off wavelength and the numerical aperture. The core radius can be calculated using equation (3.1) and the index difference is related to the NA by:

$$NA = \sqrt{n_{core}^2 - n_{clad}^2} \tag{4.1}$$

In Fig. 4.1 the gain as a function of the cut-off wavelength for ZBLAN fibres is shown for several NA's. For the simulation, the signal wavelength was chosen as 1310 nm while the pump wavelength was at its optimum of 1017 nm. The amplifier is operating in the small-signal regime (P_s = 1 μW) with a co-propagating pump power of 100 mW. The dopant concentration is 500 ppmwt. We used the material parameters of Fig. 2.2 and a background loss of 0.1 dB/m. At each cut-off wavelength the fibre length is optimised for maximum gain.

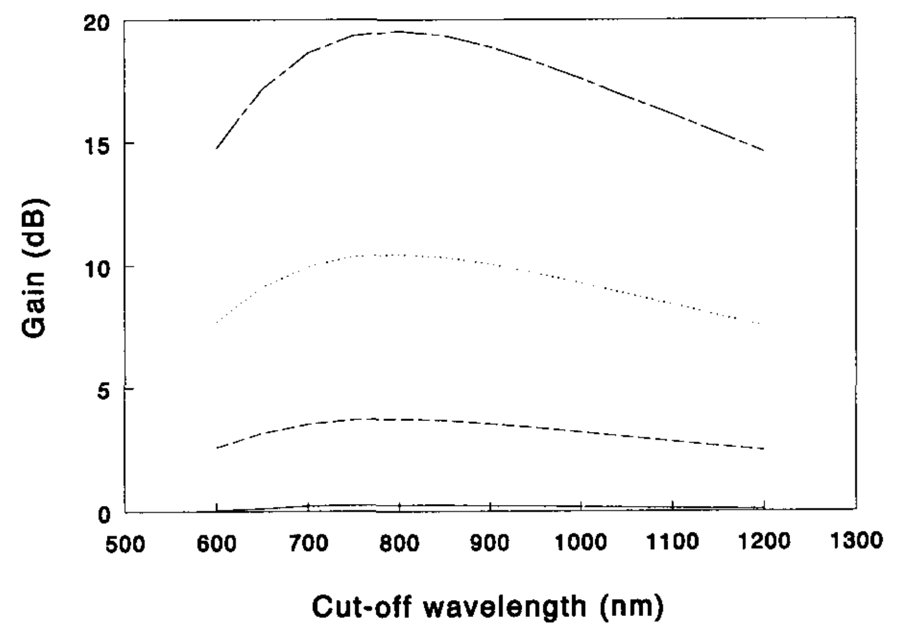

Fig. 4.1: Small-signal gain versus cut-off wavelength for ZBLAN. NA=0.1 (solid), 0.2 (dashed), 0.3 (dotted), 0.4 (dash-dotted)

From fig. 4.1 it is clear that an optimum cut-off wavelength exists. This optimum is located at approximately 800 nm and is virtually independent of the fibre NA. From the figure it is already clear that the NA must be chosen very large (See section 4.3). For cut-off wavelengths beyond 1017 nm, the fibre is no longer single-moded at the pump wavelength. The model only incorporates the fundamental mode, so the multimode part of the curve is actually not properly modelled. The optimum cut-off wavelength is a result of two effects. In fig. 3.2 an example was shown of the pump and signal modes. Because the wavelengths differ, the mode profiles will differ as well. If the cut-off wavelength is decreased from 1000 nm, the optical intensities will increase as the modes are confined to a smaller area. Furthermore, the pump and signal modes will show better overlap. This means that the fibre is not seriously being underpumped in the section close to the cladding where the signal power is still quite strong. If the cut-off wavelength is decreased too far however, a considerable part of the optical power will propagate in the undoped cladding and will not contribute to amplification.

In Fig 4.2 results are depicted for the GeGaS host material. Again, the NA varies from 0.1 to 0.4. The optimum pump wavelength is 1026 nm for this material. A background loss of 0.1 dB/m was assumed. The other conditions are the same as for ZBLAN. The gain of this fibre is considerably higher than the gain of the ZBLAN fibre. It appears to be less dependent on the cut-off wavelength. For a high NA, the gain saturates and the optimum cut-off wavelength will shift to slightly lower values. Because of the insensitivity to the cut-off wavelength, we will consider the optimum to be at 800 nm for all values of the numerical aperture, throughout the rest of our simulations. Since the gain curve is very flat for a high-NA fibre, one may consider choosing a somewhat higher cut-off wavelength. The fibre core radius will be larger, making it easier to manufacture. Furthermore, coupling to standard communication fibres will be easier and may not require special techniques for mode adaptation.

4.3 Choice of the fibre numerical aperture

Having determined the optimum cut-off wavelength, we can investigate the influence of the numerical aperture on the fibre's gain. Simulations were performed for ZBLAN and GeGaS hosts (See fig. 4.3). For both fibre types the cut-off wavelength was chosen to be 800 nm. The other parameters are: λ_s=1310 nm, λ_p=1017 nm (ZBLAN) / 1026 nm (GeGaS), P_s=1 μW, ρ=500 ppmwt. The simulation was repeated for three pump powers, 50 mW, 100 mW and 200 mW. For both hosts, the gain increases at increasing NA. It follows from (3.1) and (3.6) that the core radius a decreases, while the normalised frequency V remains the same. Using this result in (3.5), we find that the optical intensities increase with increasing NA. In fact, the shape of the mode profiles does not change as it did when the cut-off wavelength was varied. The modes are only confined to a smaller radius. In this case there are no counter-balancing effects, so the higher the NA, the higher the gain will be. This does not mean that the gain will increase without limit.

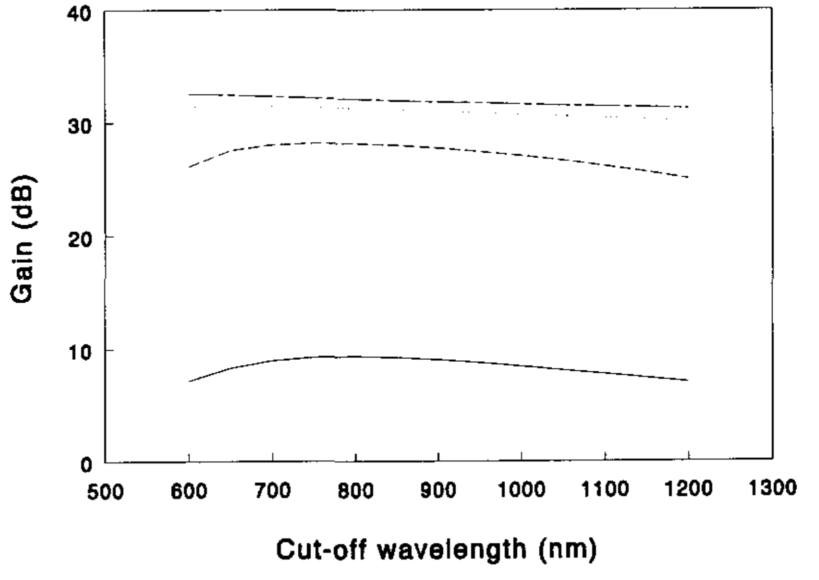

Fig. 4.2: Small-signal gain versus cut-off wavelength for GeGaS. NA=0.1 (solid), 0.2 (dashed), 0.3 (dotted), 0.4 (dash-dotted)

The gain will eventually be limited by the amount of pump power that is fed to the fibre. The fundamental limit to the gain follows from:

$$G_{max} = 10\log\left(\frac{P_p}{P_s}\frac{\lambda_p}{\lambda_s}\right) \tag{4.2}$$

For 100 mW pump this amounts to 49 dB. In practice, this limit will never be reached, because noise (ASE) is generated, which consumes part of the pump power. This is why the gain flattens for high NA values. Because of the higher efficiency of the sulfide host, the flattening will occur in an earlier stage. It is interesting to note that the ZBLAN fibre will eventually outperform the GeGaS fibre. This is probably due to strong ASE being generated in the latter fibre at wavelengths beyond 1310 nm. The optimum wavelength for amplification is at 1333 nm while for the ZBLAN fibre it is at the desired 1310 nm (See section 5.4). In practice, the numerical aperture is limited to about 0.4. Larger NA's will lead to small, unpractical core diameters. It is best to choose the NA as low as possible while the gain is still adequate. In case of GeGaS, a NA of 0.3 would be a good choice.

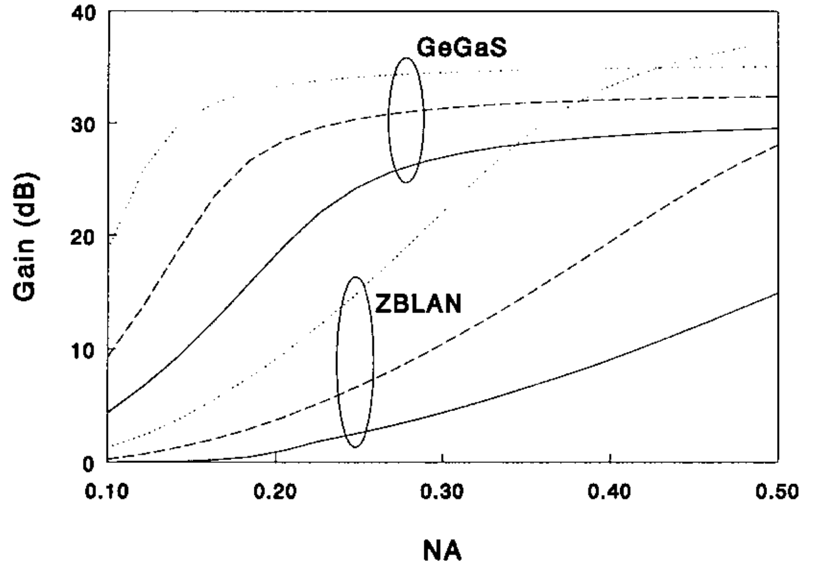

Fig. 4.3: Small-signal gain versus numerical aperture. P_p=50 mW (solid), 100 mW (dashed), 200 mW (dotted)

5. Characteristics of the Praseodymium-doped fibre amplifier

In chapter 4, a method was described to find an optimum structure for the Praseodymium-doped fibre. This was demonstrated for a typical small-signal amplifier. Actually, the fibre would have to be redesigned for each operating condition. It seems however that the optimum does not change too much with changing operating conditions. Anyhow, once a fibre structure has been chosen, we are interested in the fibre's behaviour under changing conditions. In this chapter the most important characteristics of the amplifier will be discussed, including the wavelength dependence and the saturation behaviour.

5.1 Determining the fibre length

In order to find the characteristics of a practical amplifier, the fibre length has to be determined first. The optimum length is closely related to the available pump power. The more power is available, the longer the fibre has to be in order to benefit from the extra power. This is shown in fig. 5.1, where the gain versus fibre length is shown for a 500 ppmwt ZBLAN fibre with λ_c = 800 nm and NA = 0.3. It is operated at P_s = 1 μW, λ_p = 1017 nm, λ_s = 1310 nm. The pump powers are 50 mW, 100 mW and 200 mW.

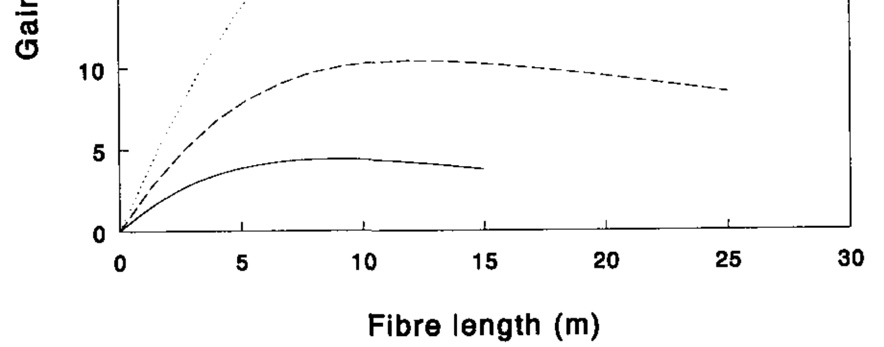

Fig. 5.1: Gain versus fibre length for ZBLAN at P_s=1 μW. P_p=50 mW (solid), 100 mW (dashed), 200 mW (dotted)

The optimum length for pump powers of 50 mW, 100 mW and 200 mW are 9 m, 12 m and 16 m respectively. If the fibre is too long, the signal will be attenuated in the last section of the fibre due to ground state absorption and background loss. Fig. 5.2 shows simulation results for an input signal power of 1 mW. This is a typical booster amplifier application. As expected, the optimum length is shifted to somewhat lower values. Due to the larger signal power, the pump power is exhausted after a shorter length.

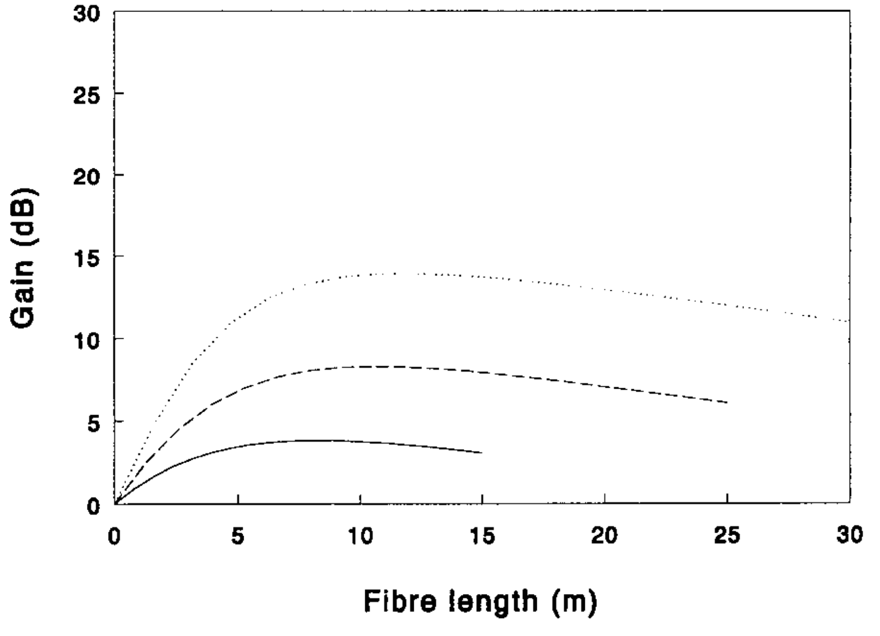

Fig. 5.2: Gain versus fibre length for ZBLAN at P_s=1 mW. P_p=50 mW (solid), 100 mW (dashed), 200 mW (dotted)

For sulfide glasses, there is no noticeable signal ground state absorption at 1.31 μm. This is why the choice of the fibre length is less critical for this material (Fig 5.3). There is only a very small decrease in gain due to the fibres background loss. The optimum is at approximately 9 meters, for all pump powers. If the fibre is used in a booster amplifier (Fig 5.4), the length can be decreased to about 6 meters, but this is not essential. For sulfide fibres, the optimum length is smaller than or equal to ZBLAN fibres. In addition to the higher gain, this can be considered as another advantage compared to ZBLAN.

5.2 Saturation in booster amplifiers

If the PDFA is used as a power booster, the input power can be quite large (-10 dBm ~ 10 dBm). In this regime, the amplifier will tend to saturate. The saturation behaviour is shown in fig. 5.5. The following parameters were used: ρ = 500 ppmwt, λ_c = 800 nm, NA = 0.3, λ_p

= 1017 nm (ZBLAN) / 1026 nm (GeGaS), λ_s = 1310 nm.

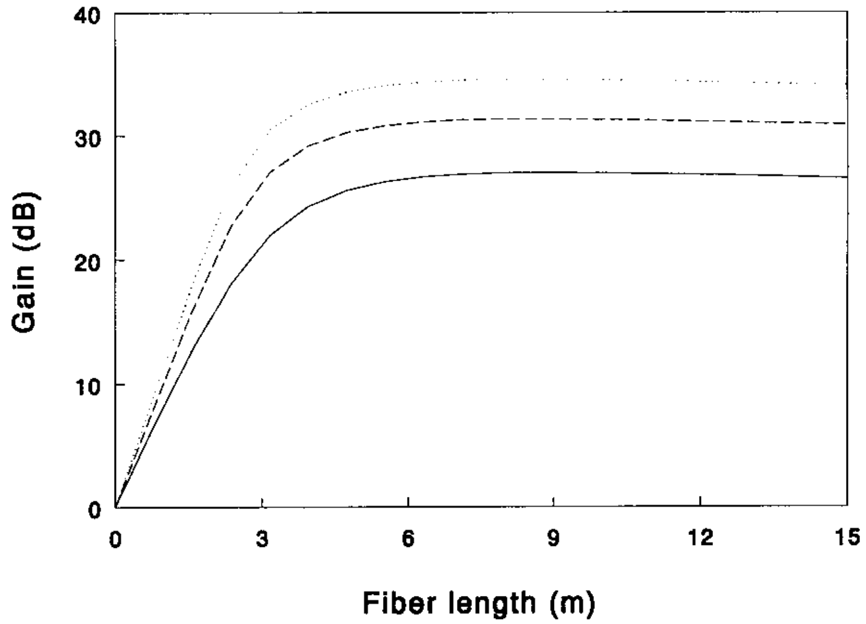

Fig. 5.3: Gain versus fibre length for GeGaS at P_s=1 μW. P_p=50 mW (solid), 100 mW (dashed), 200 mW (dotted)

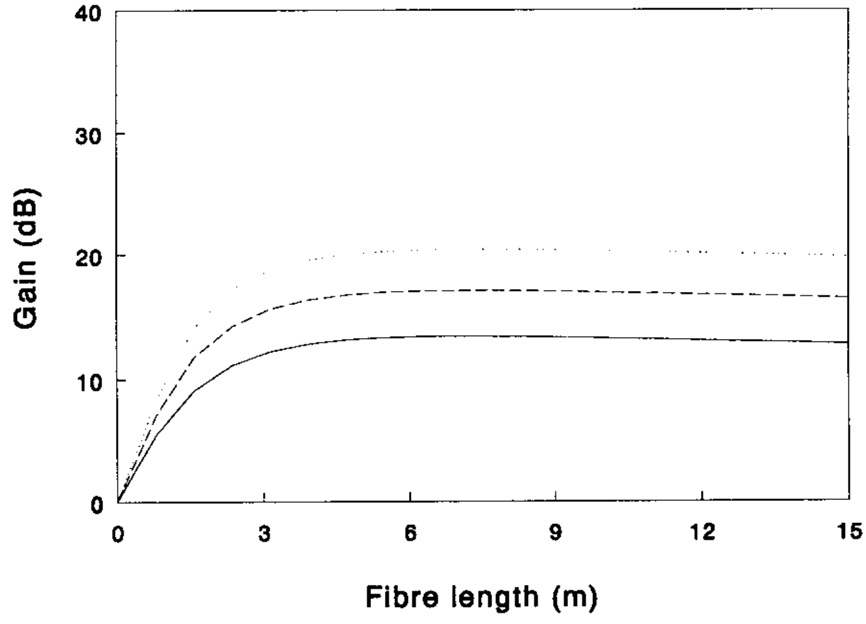

Fig. 5.4: Gain versus fibre length for GeGaS at P_s=1 mW. P_p=50 mW (solid), 100 mW (dashed), 200 mW (dotted)

The pump powers are 50, 100 and 200 mW. For each pump power, the optimum length was used, so $L = 9$ m for the sulfide fibre and $L = 9 / 12 / 16$ m for the ZBLAN fibre. At 50 mW, the saturated output power of the sulfide fibre is about 20 mW. In the saturated regime, the gain curve approaches a constant slope of -1 dB/dBm. This means that the output power is nearly independent of the input power. This is an interesting feature. The amplifier can be used to eliminate average power fluctuations at the input. Due to the slow response of the amplifier (lifetime > 100 μs), intensity-modulated signals will not be effected for modulation frequencies higher than 50 kHz [15]. In most practical systems, this condition will be satisfied.

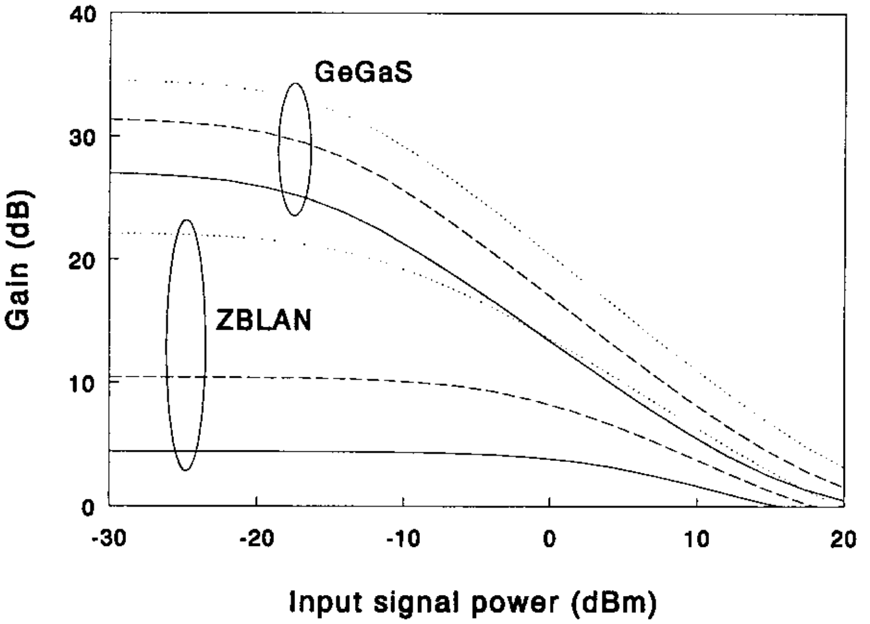

Fig. 5.5: Gain versus input signal power. P_p=50 mW (solid), 100 mW (dashed), 200 mW (dotted)

5.3 Pump power efficiency

Doped fibres for fibre amplifiers are often characterised by their pump power efficiency. This parameter can be used to gain insight in the quality of a fibre. The pump power efficiency is the slope of the gain curve versus pump power, as in fig. 5.6. The fibre length is chosen large enough, for the pump power to be completely absorbed. This yields maximum slopes. For ZBLAN we chose 20 m, and for GeGaS the length is 10 m. The other parameters are the same as before. The pump power efficiency can not be used to calculate the actual gain. For higher pump powers the amplifier will always be saturated due to ASE. The efficiency of the sulfide amplifier is a factor 6 higher than the efficiency of the ZBLAN amplifier. This is attributed to the improved lifetime, higher emission cross-section and lower ESA cross-section at 1310 nm.

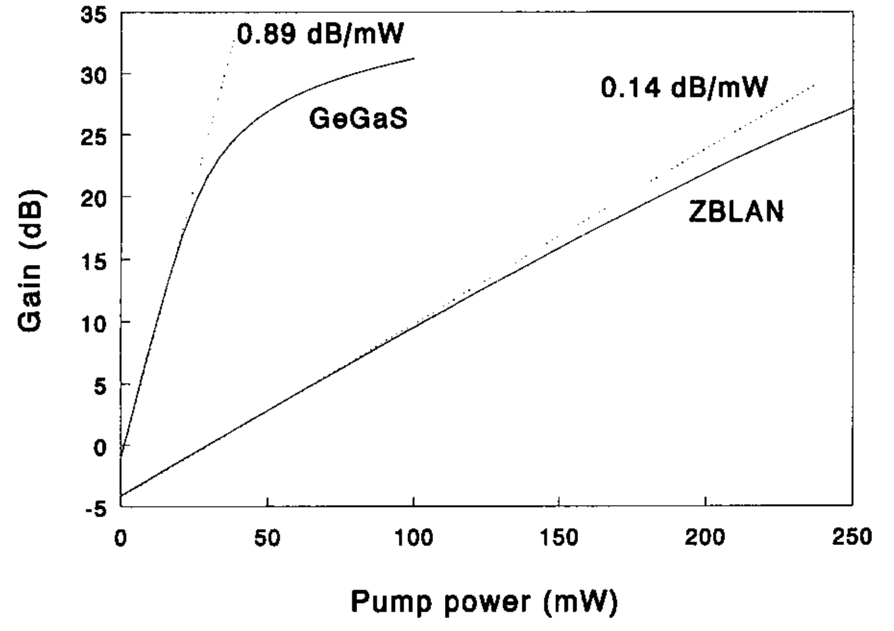

Fig. 5.6: Small-signal gain versus pump power for ZBLAN and GeGaS.

5.4 Wavelength dependence

More and more optical telecommunication links are being designed or upgraded for the implementation of WDM-transmission. This means that the capacity of a fibre is increased by the use of multiple wavelengths. If optical amplifiers are used in these systems, the wavelength dependence of these devices must be studied carefully. The choice of transmitter wavelengths depends, among other things, on the characteristics of the amplifier. Ideally the gain should be independent of the wavelength, so all channels will have the same gain. If this is not the case, equalizers may be required to eliminate the differences.

In fig 5.7 simulation results are shown of the small-signal gain versus signal wavelength. Again the fibre length is optimised for each pump power level. For the ZBLAN fibre the gain peak is at 1310 nm. The sulfide fibre amplifier has its maximum at 1333 nm. However, the gain at 1310 still strongly exceeds the gain of ZBLAN fibres. The slope at 1310 nm is about 0.75 dB/nm. In a multi-channel WDM-system this may result in several dB's difference in gain between the two outmost channels. Furthermore the gain-slope can lead to distortion in analogue CATV distribution systems, due to laser-chirping [16].

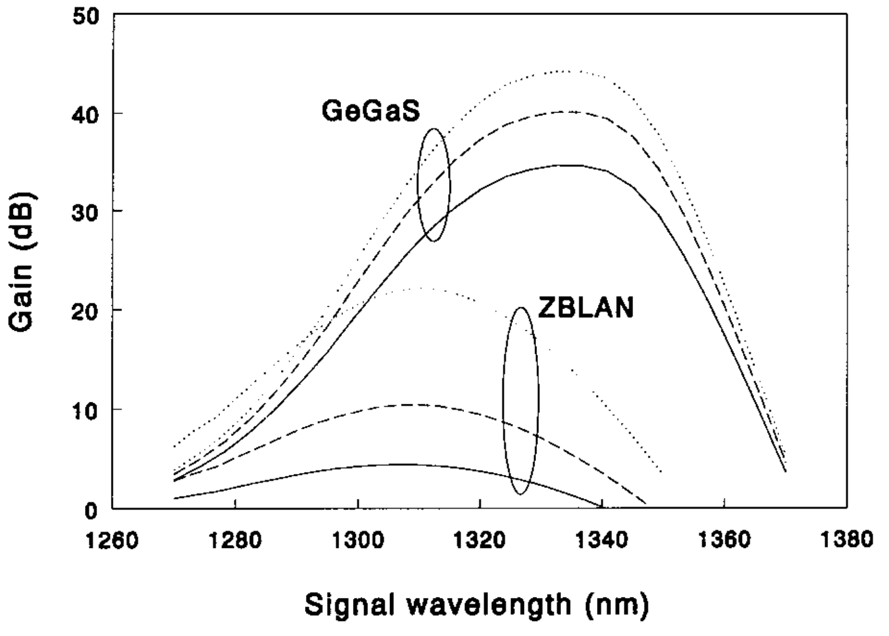

Fig. 5.7: Small-signal gain versus signal wavelength for ZBLAN and GeGaS. P_p=50 mW (solid), 100 mW (dashed), 200 mW (dotted)

The wavelength dependence of the PDFA used as booster amplifier is shown in fig. 5.8. A pump power of 100 mW was used for the simulation. For the GeGaS amplifier the gain curve is flattened with increasing input signal power. At an input power of 1 mW, the lower -3dB point is at 1292 nm. In the range 1305-1315 nm, the gain is exceptionally flat.

5.5 Influence of background loss

The fibre background loss must be kept low during the fibre fabrication process. For ZBLAN fibres it can be as low as 0.1 dB/m. In the previous simulations, the same loss was assumed for GeGaS fibres. Because no fibres have been drawn yet, it is not clear if this is feasible. Simulations using different background losses are shown in fig 5.9. The fibre length was optimised for each background loss. For background losses of 0.1 dB/m, 1 dB/m, 2 dB/m and 3 dB/m the lengths were 9 m, 5 m, 4m and 3 m respectively. Since both pump and signal beams are attenuated, the background loss is expected to cause a double decrease in gain. The results show that this is not the case, because the optimum length decreases for higher background losses. For losses as high as 3 dB/m the sulfide amplifier performs better than the ZBLAN amplifier, at 1310 nm.

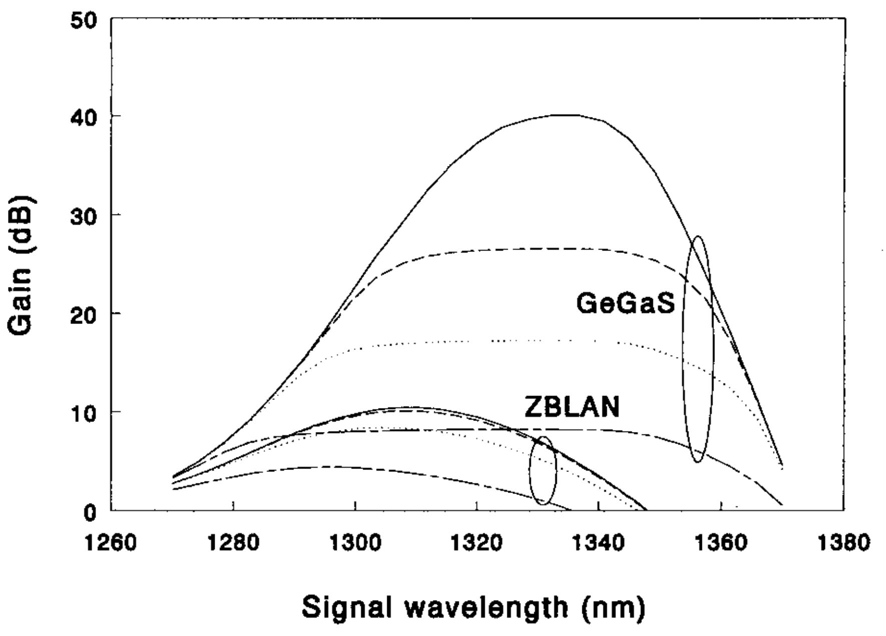

Fig. 5.8: Gain versus signal wavelength for saturated ZBLAN and GeGaS amplifiers. P_s=1 μW (solid), 100 μW (dashed), 1 mW (dotted), 10 mW (dash-dotted)

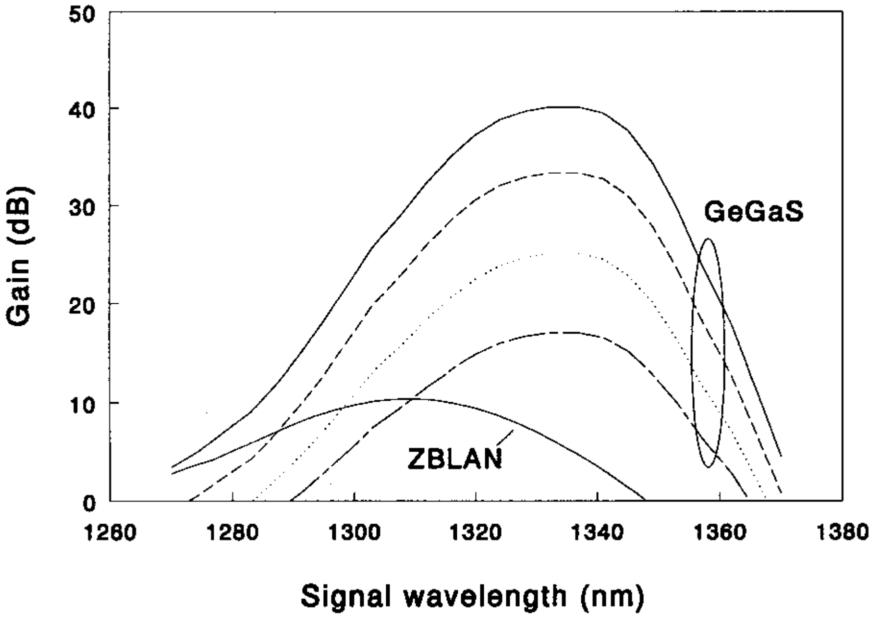

Fig. 5.9: Small-signal gain versus signal wavelength for GeGaS host at different background losses compared to a typical ZBLAN host. α=0.1 dB/m (solid), 1 dB/m (dashed), 2 dB/m (dotted), 3 dB/m (dash-dotted)

6. Experimental setup of Pr^{3+}-doped fibre amplifier

At the Telecommunications Division of the Eindhoven University of Technology an experimental setup of a PDFA is built. Thanks to the kind cooperation of British Telecom and Galileo Electro Optics we have two different Praseodymium-doped fluoride fibres at our disposal. The first fibre is 13.5 m long and is doped with 760 ppmwt Pr^{3+}. The numerical aperture of the fibre is 0.4 at a cut-off wavelength of 900 nm. The background loss is 0.1 dB/m. Both ends of the fibre were already glue-spliced to a high-NA fibre. The splice losses are about 0.4 dB each. The high-NA fibres are spliced to a tapered standard fibre, each having a loss of only 0.25 dB. A additional piece of fibre of 7.5 m is available for characterisation measurements. It can be used to determine cross-section spectra and the spontaneous emission lifetime. There is also a 10 m piece of 1000 ppmwt Pr^{3+}-doped fibre available with $NA = 0.39$ and $\lambda_c = 870$ nm. This fibre has not yet been spliced.

The Pr^{3+}-doped fibres are used in the setup of fig. 6.1. The amplifier is bi-directionally pumped by two 1017 nm pump laser diodes. Each laser-chip has a maximum output power of 100 mW. About half of this power will be available for pumping, because the lasers must be pig-tailed first. Two 1017 nm/1300 nm WDM couplers are used to combine the pump and signal beams. The insertion losses of the pump and signal beams are 0.6 dB and 0.3 dB, respectively. Considering all insertion and splice losses, we expect that about 30 mW of pump power can be coupled to the Pr^{3+}-doped fibre at each end.

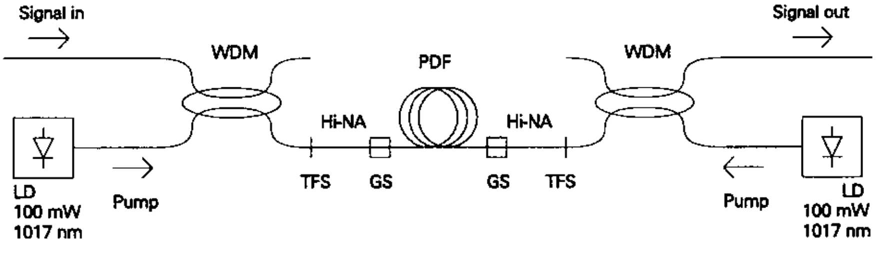

Fig. 6.1: Experimental PDFA setup. WDM: Wavelength Division Multiplexer, LD: Laser Diode, TFS: Tapered Fusion Splice, Hi-NA: High-NA fibre, GS: Glue Splice, PDF: Praseodymium-Doped Fibre

In fig. 6.2 simulation results are shown for the 760 ppmwt Pr^{3+}-doped fibre. We used the fibre parameters mentioned above in combination with the ZBLAN cross-sections and lifetime of [2,3]. The signal wavelength was 1.31 μm. For accurate results, the cross-sections and lifetime should be measured on this specific fibre, because they depend on the exact glass composition. Nevertheless, the given glass properties can be used as a first estimate. The pump power efficiency of the amplifier is 0.24 dB/mW, which corresponds to the value reported in [4] for a bi-directionally pumped PDFA using a fibre with $NA = 0.42$.

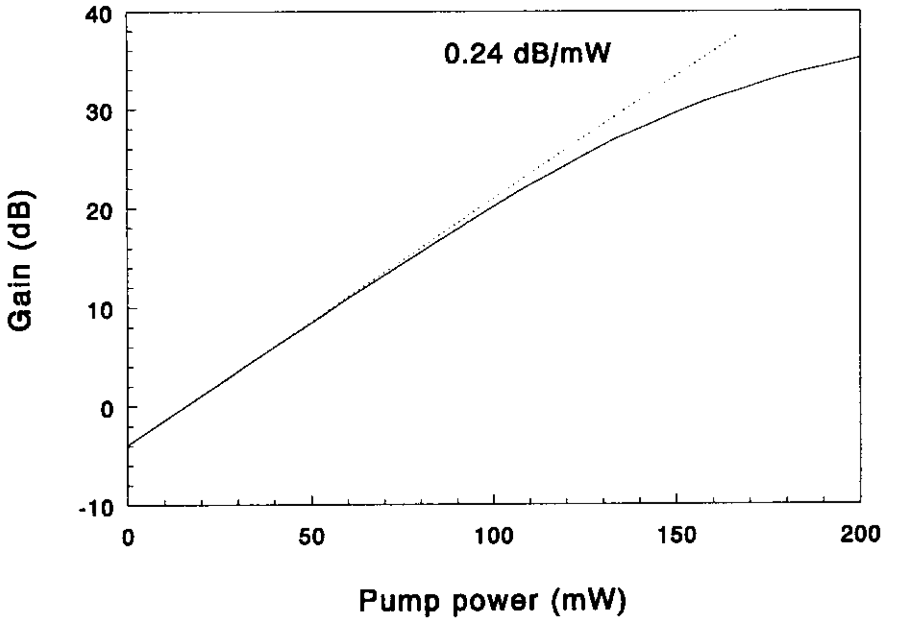

Fig. 6.2: Small-signal gain of the PDFA setup versus total coupled pump power

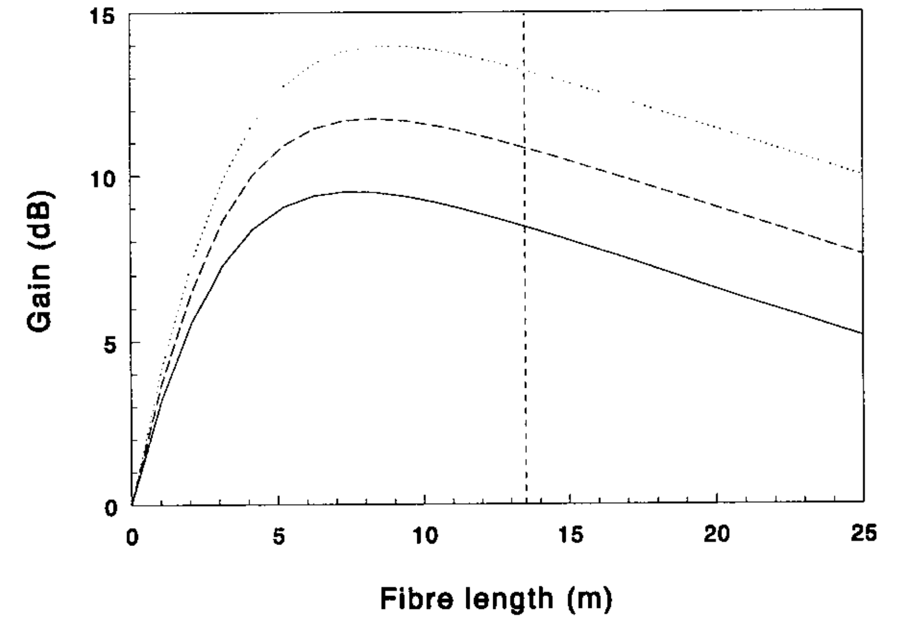

Fig. 6.3: Small-signal gain of PDFA setup versus fibre length. P_p=50 mW (solid), 60 mW (dashed), 70 mW (dotted)

In fig. 6.3 the gain versus fibre length is depicted for three pump power levels. At the estimated maximum pump power of 60 mW, the optimum fibre length would be 8.5 m. Using the 13.5 m fibre, the gain is only 0.9 dB below the optimum. We can therefore expect a gain of about 11 dB.

The simulation results presented in this report indicate that Pr^{3+}-doped sulfide glasses have very promising optical properties to be used in a PDFA. At present, the feasibility of manufacturing Praseodymium-doped sulfide fibres is being investigated. Hopefully, good fibres will become available in the future to be implemented in the setup. Gains of more than 25 dB may then be possible, using the same setup.

7. Conclusions

While optical amplifiers for the 1.55 μm window are commonly being used, amplifiers for the 1.3 μm window are still in development. The introduction of fibre amplifiers for this wavelength proved to be much more difficult. Until recently, all Praseodymium-doped fibre amplifiers were based on ZBLAN glasses. The performance of these glasses is limited due to the low quantum efficiency. Today, new host materials are being developed with substantially improved properties. For the GeGaS-based glasses, the emission lifetime is more than three times higher than the lifetime in ZBLAN hosts. The stimulated emission cross-section is higher too, but is shifted to longer wavelength. GeGaS glasses are less hampered by excited state absorption than ZBLAN hosts.

To compensate for limited fibre efficiency, complex amplifier setups can be used. Using a bidirectionally pumped amplifier in combination with polarisation multiplexing of the pump lasers, the effective pump power can virtually be quadrupled. If a double-path configuration is employed, the gain is doubled once more.

To predict amplifier performance, a mathematical model is used which includes excited state absorption, ground state absorption and background loss. The model incorporates the distribution of the optical modes across the fibres cross-section. Also, all forward and backward travelling noise is included. The model is solved numerically on a computer system. Results from simulations agreed well with measurements found in literature.

Simulations showed that the optimum cut-off wavelength for Praseodymium-doped fibres is 800 nm for ZBLAN as well as for sulfide hosts. Using ZBLAN, the numerical aperture must be very high to produce efficient fibres. For sulfide fibres no noteworthy increase in gain is expected by increasing the NA beyond 0.3. At NA = 0.3, the cut-off wavelength can be chosen higher than 800 nm without sacrificing too much gain. The combination of high cut-off wavelength and low NA results in a larger core diameter, facilitating fibre fabrication and decreasing coupling losses to standard fibre.

Thanks to the improved efficiency, sulfide fibres can be shorter than ZBLAN fibres, especially for higher pump powers. A small-signal gain of more than 25 dB at 1310 nm is expected, for pump powers as low as 50 mW. For ZBLAN fibres, more than 200 mW is needed for this. Both ZBLAN and sulfide amplifiers are saturated by applying a large input signal power. In fact, in this regime the output power will be virtually independent of the input power. At 1310 nm, the pump power efficiency of sulfide fibres is a factor 6 higher (0.89 dB/mW) than for ZBLAN fibres. The sulfide amplifier has its gain maximum at 1333 nm, at an optimum pump wavelength of 1026 nm. The steep slope in the gain curve at 1310 nm will lead to different gains for each channel in a WDM-system. In a booster amplifier the gain is extremely flat within a spectral range of several nanometers.

We found that the background loss of GeGaS fibres has less impact on the gain than expected. If the background loss is inreased from 0.1 dB/m to 1.0 dB/m the gain will decrease by 6 dB, still giving 25 dB gain at 100 mW pump power.

A setup of the bi-directionally pumped PDFA is being constructed using two pump lasers of 100 mW (chip output) each. In this setup Pr^{3+}-doped fluoride fibres are used. Simulation results predict a small-signal gain of about 11 dB at 1310 nm, assuming that 30 mW can be coupled into the doped fibre at each end. The pump power efficiency is 0.24 dB/mW.

References

[1] Artiglia, M. and P. di Vita, M. Potenza.
Optical fibre amplifiers: Physical model and design issues.
Opt. Quantum Electron., vol. 26(1994), p. 585-608

[2] Quimby, R.S. and B. Zheng.
New excited-state absorption measurement technique and application to Pr^{3+} doped fluorozirconate glass.
Appl. Phys. Lett., vol. 60(1992), no. 2, p. 1055-1057

[3] Pedersen, B. and W.J. Miniscalco, R.S. Quimby.
Optimization of Pr^{3+}:ZBLAN fiber amplifiers.
Phot. Techn. Lett., vol. 4(1992), no. 5, p. 446-448

[4] Ohishi, Y. and T. Kanamori, M. Shimizu, M. Yamada, Y. Terunuma, J. Temmyo, M. Wada, S. Sudo.
Praseodymium-Doped Fiber Amplifiers at 1.3 μm.
IEICE Trans. Commun., vol. E77-B(1994), no. 4, p. 421-439

[5] Simons, D.R. and A.J. Faber, H. de Waal.
Pr^{3+}-doped GeS_x-based glasses for fiber amplifiers at 1.3 μm.
Opt. Lett., vol. 20(1995), no. 5, p. 468-470

[6] Simons, D.R., Private communication.

[7] Hanafusa, H. and M. Horiguchi, J. Noda.
Thermally-diffused expanded core fibres for low-loss and inexpensive photonic components.
Electr. Lett., vol. 27(1991), no. 21, p. 1968-1969

[8] Yamada, M. and M. Shimizu, Y. Ohishi, J. Temmyo, T. Kanamori, S. Sudo.
Highly efficient configuration of a Pr^{3+}-doped fluoride fiber amplifier module with an optical circulator.
Phot. Techn. Lett., vol. 5(1993), no. 9, p. 1011-1013

[9] Osch, A.W.H. van.
Measurements and models on an erbium-doped fibre amplifier.
Eindhoven University of Technology,
Faculty of electrical engineering, Telecommunications division, 1994.
Graduation report nr. 7190

[10] Giles, C.R. and E. Desurvire.
Modeling Erbium-doped fiber amplifiers.
J. Lightwave Technol., vol. 9(1991), no. 2, p. 271-283

[11] Jeunhomme, L.B.
Single-mode fiber optics: Principles and applications.
New York: Marcel Dekker, 1983.

[12] Karasek, M. and H. Többen.
Theoretical comparison of Pr^{3+}-doped La-Ga-S and fluoride glass fibre amplifiers.
Radioengineering, vol. 2(1993), no. 3, p. 21-25

[13] Miyajima, Y. and T. Sugawa, Y. Fukasaku.
38.2 dB amplification at 1.31 μm and possibility of 0.98 μm pumping in Pr^{3+}-doped fluoride fibre.
Electr. Lett., vol. 27(1991), no. 19, p. 1706-1707

[14] Ohishi, Y. and T. Kanamori, T. Nishi, S. Takahashi, E. Snitzer.
Concentration effect on gain of Pr^{3+}-doped fluoride fiber for 1.3 μm amplification.
Phot. Techn. Lett., vol. 4(1992), no. 12, p. 1338-1341

[15] Karasek, M.
Analysis of Gain Dynamics in Pr^{3+}-doped fluoride fiber amplifiers.
Phot. Techn. Lett., vol. 7(1995), no. 3, p. 299-302

[16] Clesca, B. and P. Bousselet, L. Hamon.
Second-order distortion improvements or degradations brought by erbium-doped fiber amplifiers in analog links using directly modulated lasers.
Phot. Techn. Lett., vol. 5(1993), no. 9, p. 1029-1031

List of abbreviations

ASE	Amplified Spontaneous Emission
CATV	Cable Television
EDFA	Erbium-Doped Fibre Amplifier
ESA	Excited-State Absorption
FTTH	Fibre To The Home
GS	Glue Splice
GSA	Ground-State Absorption
Hi-NA	High Numerical Aperture fibre
LD	Laser Diode
MFD	Mode Field Diameter
MR	Mirror
NA	Numerical Aperture
OC	Optical Circulator
OFA	Optical Fibre Amplifier
OTDM	Optical Time Domain Multiplexing
PDF	Praseodymium-Doped Fibre
PDFA	Praseodymium-Doped Fibre Amplifier
PM	Polarisation Multiplexer
PON	Passive Optical Network
SOA	Semiconductor Optical Amplifier
TEC	Thermally-diffused Expanded Core splice
TFS	Tapered Fusion Splice
WDM	Wavelength Division Multiplexer/multiplexing
ZBLAN	ZrF_4-BaF_2-LaF_3-AlF_3-NaF

List of symbols

Constants

c	Speed of light in vacuum = $2.99792 \cdot 10^{8}$	[m/s]
h	Planck's constant = $6.62559 \cdot 10^{-34}$	[Js]

Variables

a	Radius of fibre core	[m]
g_a	Signal excited-state absorption factor	[Np/m]
g_e	Signal stimulated emission factor	[Np/m]
g_g	Signal ground-state absorption factor	[Np/m]
g_p	Pump absorption factor	[Np/m]
G_{max}	Gain of an ideal optical fibre amplifier	[dB]
I	Normalised optical intensity	[m^{-2}]
L	Fibre length	[m]
NA	Numerical Aperture	[]
n_{clad}	Refractive index of fibre cladding	[]
n_{core}	Refractive index of fibre core	[]
P	Optical power spectral density	[W/Hz]
P_{ase}^{+}	Power spectral density of co-propagating ASE	[W/Hz]
P_{ase}^{-}	Power spectral density of counter-propagating ASE	[W/Hz]
P_p	Pump power	[W]
P_p^{+}	Co-directional pump power	[W]
P_p^{-}	Counter-directional pump power	[W]
$P_{p,in}$	Input pump power	[W]
P_s	Signal power	[W]
$P_{s,in}$	Input signal power	[W]
r	Radial coordinate	[m]
V	Normalised frequency	[]
W_{IK}	Transition rate between levels I and K	[s^{-1}]
W_{03}	Pump absorption rate	[s^{-1}]
W_{31}	Signal stimulated emission rate	[s^{-1}]
W_{34}	Signal excited-state absorption rate	[s^{-1}]

x,y	Transverse coordinates	[m]
z	Longitudal coordinate	[m]
α	Background loss	[Np/m]
γ	Co-propagating fraction of total pump power	[]
ΔE	Energy gap between two electron-levels	[J]
$\Delta\nu$	Bandwidth of wavelength section	[Hz]
η_0	Density of Praseodymium atoms in the ground state	[m^{-3}]
η_3	Density of Praseodymium atoms in the excited state	[m^{-3}]
λ	Wavelength of lightwave	[m]
λ_c	Cut-off wavelength	[m]
λ_{max}	Upper wavelength bound for ASE	[m]
λ_{min}	Lower wavelength bound for ASE	[m]
λ_p	Pump wavelength	[m]
λ_s	Signal wavelength	[m]
ν	Frequency of lightwave	[Hz]
ν_p	Frequency of pump	[Hz]
ν_s	Frequency of signal	[Hz]
ρ	Praseodymium concentration	[m^{-3}]
σ_{IK}	Cross-section of transition from level I to level K	[m^2]
σ_{02}	Signal ground-state absorption cross-section	[m^2]
σ_{03}	Pump absorption cross-section	[m^2]
σ_{31}	Signal stimulated emission cross-section	[m^2]
σ_{34}	Signal excited-state absorption cross-section	[m^2]
τ	Spontaneous emission lifetime	[s]
τ_I	Spontaneous emission lifetime of level I	[s]

(268) Boom, H. van den and W. van Etten, W.H.C. de Krom, P. van Bennekom, F. Huijskens, L. Niessen, F. de Leijer
AN OPTICAL ASK AND FSK PHASE DIVERSITY TRANSMISSION SYSTEM.
EUT Report 92-E-268. 1992. ISBN 90-6144-268-0

(269) Putten, P.H.A. van der
MULTIDISCIPLINAIR SPECIFICEREN EN ONTWERPEN VAN MICROELEKTRONICA IN PRODUKTEN (in Dutch).
EUT Report 93-E-269. 1993. ISBN 90-6144-269-9

(270) Bloks, R.H.J.
PROGRIL: A language for the definition of protocol grammars.
EUT Report 93-E-270. 1993. ISBN 90-6144-270-2

(271) Bloks, R.H.J.
CODE GENERATION FOR THE ATTRIBUTE EVALUATOR OF THE PROTOCOL ENGINE GRAMMAR PROCESSOR UNIT.
EUT Report 93-E-271. 1993. ISBN 90-6144-271-0

(272) Yan, Keping and E.M. van Veldhuizen
FLUE GAS CLEANING BY PULSE CORONA STREAMER.
EUT Report 93-E-272. 1993. ISBN 90-6144-272-9

(273) Smolders, A.B.
FINITE STACKED MICROSTRIP ARRAYS WITH THICK SUBSTRATES.
EUT Report 93-E-273. 1993. ISBN 90-6144-273-7

(274) Bollen, M.H.J. and M.A. van Houten
ON INSULAR POWER SYSTEMS: Drawing up an inventory of phenomena and research possibilities.
EUT Report 93-E-274. 1993. ISBN 90-6144-274-5

(275) Deursen, A.P.J. van
ELECTROMAGNETIC COMPATIBILITY: Part 5, installation and mitigation guidelines, section 3, cabling and wiring.
EUT Report 93-E-275. 1993. ISBN 90-6144-275-3

(276) Bollen, M.H.J.
LITERATURE SEARCH FOR RELIABILITY DATA OF COMPONENTS IN ELECTRIC DISTRIBUTION NETWORKS.
EUT Report 93-E-276. 1993. ISBN 90-6144-276-1

(277) Weiland, Siep
A BEHAVIORAL APPROACH TO BALANCED REPRESENTATIONS OF DYNAMICAL SYSTEMS.
EUT Report 93-E-277. 1993. ISBN 90-6144-277-X

(278) Gorshkov, Yu.A. and V.I. Vladimirov
LINE REVERSAL GAS FLOW TEMPERATURE MEASUREMENTS: Evaluations of the optical arrangements for the instrument.
EUT Report 93-E-278. 1993. ISBN 90-6144-278-8

(279) Creyghton, Y.L.M. and W.R. Rutgers, E.M. van Veldhuizen
IN-SITU INVESTIGATION OF PULSED CORONA DISCHARGE.
EUT Report 93-E-279. 1993. ISBN 90-6144-279-6

(280) Li, H.Q. and R.P.P. Smeets
GAP-LENGTH DEPENDENT PHENOMENA OF HIGH-FREQUENCY VACUUM ARCS.
EUT Report 93-E-280. 1993. ISBN 90-6144-280-X

(281) Di, Chennian and Jochen A.G. Jess
ON THE DEVELOPMENT OF A FAST AND ACCURATE BRIDGING FAULT SIMULATOR.
EUT Report 94-E-281. 1994. ISBN 90-6144-281-8

(282) Falkus, H.M. and A.A.H. Damen
MULTIVARIABLE H-INFINITY CONTROL DESIGN TOOLBOX: User manual.
EUT Report 94-E-282. 1994. ISBN 90-6144-282-6

(283) Meng, X.Z. and J.G.J. Sloot
THERMAL BUCKLING BEHAVIOUR OF FUSE WIRES.
EUT Report 94-E-283. 1994. ISBN 90-6144-283-4

(284) Rangelrooij, A. van and J.P.M. Voeten
CCSTOOL2: An expansion, minimization, and verification tool for finite state CCS descriptions.
EUT Report 94-E-284. 1994. ISBN 90-6144-284-2

(285) Roer, Th.G. van de
MODELING OF DOUBLE BARRIER RESONANT TUNNELING DIODES: D.C. and noise model.
EUT Report 95-E-285. 1995. ISBN 90-6144-285-0

(286) Dolmans, G.
ELECTROMAGNETIC FIELDS INSIDE A LARGE ROOM WITH PERFECTLY CONDUCTING WALLS.
EUT Report 95-E-286. 1995. ISBN 90-6144-286-9

(287) Liao, Boshu and P. Massee
RELIABILITY ANALYSIS OF AUXILIARY ELECTRICAL SYSTEMS AND GENERATING UNITS.
EUT Report 95-E-287. 1995. ISBN 90-6144-287-7

(288) Weiland, Siep and Anton A. Stoorvogel
OPTIMAL HANKEL NORM IDENTIFICATION OF DYNAMICAL SYSTEMS.
EUT Report 95-E-288. 1995. ISBN 90-6144-288-5

(289) Konieczny, Pawel A. and Lech Józwiak
MINIMAL INPUT SUPPORT PROBLEM AND ALGORITHMS TO SOLVE IT.
EUT Report 95-E-289. 1995. ISBN 90-6144-289-3

(290) Voeten, J.P.M.
POOSL: An object-oriented specification language for the analysis and design of hardware/software systems.
EUT Report 95-E-290. 1995. ISBN 90-6144-290-7

(291) Smeets, B.H.T. and M.H.J. Bollen
STOCHASTIC MODELLING OF PROTECTION SYSTEMS: Comparison of four mathematical techniques.
EUT Report 95-E-291. 1995. ISBN 90-6144-291-5

(292) Voeten, J.P.M. and A. van Rangelrooij
CCS AND TIME: A practical and comprehensible approach to a performance evaluation of finite state CCS descriptions.
EUT Report 95-E-292. 1995. ISBN 90-6144-292-3

(293) Voeten, J.P.M.
SEMANTICS OF POOSL: An object-oriented specification language for the analysis and design of hardware/software systems.
EUT Report 95-E-293. 1995. ISBN 90-6144-293-1

(294) Osch, A.W.H. van
MODELLING OF PRASEODYMIUM-DOPED FLUORIDE AND SULFIDE FIBRE AMPLIFIERS FOR THE 1.3 μM WAVELENGTH REGION.
EUT Report 95-E-294. 1995. ISBN 90-6144-294-X